

ELASTOPLASTICALLY ACCOMMODATED HYDRIDE FORMATION AND EMBRITTLEMENT

J. Lufrano, P. Sofronis* and H. K. Birnbaum

University of Illinois at Urbana-Champaign

Materials Research Laboratory

104 South Goodwin Avenue

Urbana, Illinois 61801

February 1997

* Corresponding author.

ABSTRACT

In a previous work, the authors (1996) investigated stress driven diffusion of hydrogen in a hydride forming system whose constitutive response was modeled as linearly elastic. In the present work the more realistic constitutive assumption of a purely elastic hydride accommodated elastoplastically by the surrounding matrix is used. Due to the nonlinearity in the material deformation, the classical description and calculation of the *accommodation energy* of formation and *interaction energy* with an external stress using Eshelby's methodology are no longer valid. The elastoplastic deformation of the matrix due to the volume dilatation induced by the hydride and the interaction of this deformation with externally applied stresses are studied. The energetics of the hydride formation is revisited and the terminal solid solubility of hydrogen in solution is defined on the basis of the total elastoplastic work done on the system by the forming hydride and the external loads. Hydrogen diffusion and hydride formation coupled with the elastoplastic deformation of the material are modeled at a blunting crack tip in the case of the niobium-hydrogen system. Nonlinear finite element analysis is used to monitor the local distribution and time evolution of hydrogen concentration, hydride volume fraction, stress and strain as the externally applied loads increase. A Griffith fracture criterion allows the calculation of a critical hydride size in the neighborhood of the crack tip at which cracking of the hydride particle by the local stresses is energetically favorable. Using this criterion for fracture initiation, one can predict the reduced fracture resistance of hydride forming systems quantitatively and investigate the fracture toughness dependence of the material on initial concentration and loading rate.

1. INTRODUCTION

In a previous work the authors (1996) reviewed the mechanism of hydride formation and cracking for hydrogen embrittlement, and modeled the phenomenon from a continuum mechanics viewpoint in an isotropic, linearly elastic material. The present study is concerned with transient hydrogen diffusion and hydride formation and cracking in an elastoplastically deforming material.

When a crack in an elastoplastic material is loaded under plane strain, mode I conditions the hydrostatic stress in front of the crack becomes increasingly tensile causing the chemical potential of the hydrogen in solid solution to decrease and lowering the terminal solid solubility of the hydrogen in solution. The gradients in the chemical potential of the hydrogen in solid solution drive the diffusion of hydrogen from areas distant from the crack toward the crack tip. If the local concentration of hydrogen in front of the crack reaches the level of the stress reduced solvus concentration, precipitation of hydride becomes energetically favorable. Since the hydride phase is extremely brittle, with fracture toughness of the order of $1 \text{ MPa}\sqrt{\text{m}}$ (Simpson and Puls, 1979; Gahr et al., 1980), a cleavage crack propagates through until it reaches the higher toughness solid solution. Formation of new hydride in front of the advancing crack will lead to failure through a repeating process of stress induced hydride formation and cleavage (Westlake, 1969; Birnbaum, 1984, 1990).

In the authors' (1996) previous work, the terminal solid solubility (TSS) in front of a crack (the local solvus concentration), c_s^σ , hydrogen atoms per solute atom, was calculated in a material under external stress by

$$c_s^\sigma = A \exp\left(\frac{H_h}{RT}\right) \exp\left(\frac{W_{\text{acc}}}{RT}\right) \exp\left(\frac{W_{\text{int}}}{RT}\right), \quad (1)$$

where the accommodation energy, W_{acc} , per mole of hydride formed in the absence of the external stress and the interaction energy W_{int} of the formed hydride with the external stress were determined using elastic principles (Eshelby, 1956, 1957; Birnbaum et al., 1976; Grossbeck and Birnbaum, 1977; Gahr and Birnbaum, 1978; Flanagan et al., 1981; Puls, 1981, 1984). In (1), A is a constant determined experimentally, R is the gas constant, T is the temperature, and the parameter H_h , which is negative, is the molal enthalpy change for transferring hydrogen from the solid solution to the hydride in the absence of any accommodation or any externally applied stress. However, since the volume increase associated with hydride formation is of the order of 10–20 percent (Puls, 1981, 1984), most metals deform plastically to allow for the accommodation of the large volume change (Birnbaum et al., 1976; Makenas and Birnbaum, 1980; Birnbaum, 1990).

Many researchers have discussed the energy of accommodation in the case of a plastically deforming matrix (Lee et al., 1980; Earmme et al., 1981; Leitch and Puls, 1992; Sen et al., 1996). Lee et al., calculated the energy of a misfitting spherical precipitate assuming ideal plastic response. Earmme et al., extended the previously mentioned work and calculated the energy of a misfitting spherical precipitate assuming either linear or power law hardening. In a comprehensive study, Leitch and Puls used finite element techniques to calculate the accommodation energy of isotropically and anisotropically misfitting oblate spheroids in an elastic perfectly plastic matrix. Sen et al., also using finite element techniques, considered the effect of different transformation paths on the accommodation energy of a misfitting spherical precipitate in a linear strain hardening material.

Another essential component of the total energy of hydride formation is the interaction energy, which is due to the interaction of the volume

change accompanying the hydride formation with an external stress field. The effect of an external stress field on the terminal solid solubility has been experimentally measured (Westlake, 1969; Birnbaum et al., 1976; Grossbeck and Birnbaum, 1977) and theoretically analyzed (Gahr et al., 1977; Grossbeck and Birnbaum, 1977; Pardee and Paton, 1980; Puls, 1981; Flanagan et al., 1981). However, these analyses are based on essentially elastic principles. Furthermore, the validity of calculating the total energy of formation by using an elastoplastic accommodation energy and an elastic interaction energy is questionable, as will be discussed in the next section.

In the current treatment of the problem, the constitutive material behavior is modeled as isotropically linear in the elastic regime and is characterized by the Prandtl-Reuss equations in the plasticity regime. The determination of the hydrogen solvus concentration is revisited and elastoplastic principles are used to calculate the total mechanical energy of hydride formation. An investigation of the hydrogen diffusion and hydride formation near a blunting crack tip in an elastoplastic material is conducted using both elastic and elastoplastic calculations of the solvus to illustrate the effects of plasticity. Formation of hydride is modeled in a probabilistic manner and does not address the issues associated with hydride shapes or the kinetics of the formation of an actual hydride particle. These calculations yield a point density of the hydride, which will be referred as the local hydride volume fraction, i.e., the probability of finding a hydride particle at a given location. A full transient finite element analysis allows for the numerical monitoring of stresses, strains, hydrogen distributions, and the expansion of the hydride zone. A Griffith fracture criterion based on the brittle cleavage of the formed hydride is proposed to assess the reduced fracture toughness observed in these systems.

2. ENERGETICS OF HYDRIDE FORMATION

One may recast (1) as

$$c_s^\sigma = B \exp \left(\frac{\Delta G_{\alpha-\beta}^{\text{tot}}}{RT} \right), \quad (2)$$

where B is an experimentally determined constant and $\Delta G_{\alpha-\beta}^{\text{tot}}$ is the Gibbs free energy change in forming a mole of hydride phase β from solid solution phase α . The Gibbs free energy change can be generally written

$$\Delta G_{\alpha-\beta}^{\text{tot}} = \Delta G_{\alpha-\beta}^{\text{chem}} + \Delta G_{\alpha-\beta}^{\text{sur}} + \Delta G_{\alpha-\beta}^{\text{mech}}, \quad (3)$$

where $\Delta G_{\alpha-\beta}^{\text{chem}}$ is the chemical Gibbs energy change, in the hydride formation, $\Delta G_{\alpha-\beta}^{\text{sur}}$ is the free energy needed for the creation of the interface and $\Delta G_{\alpha-\beta}^{\text{mech}}$ is the total mechanical free energy of hydride formation. For hydride formation with purely elastic accommodation (Birnbaum, Grossbeck and Amano, 1976) the free energy of formation is written as

$$\Delta G_{\alpha-\beta}^{\text{tot}} = \Delta G_{\alpha-\beta}^{\text{chem}} + \Delta G_{\alpha-\beta}^{\text{sur}} + \Delta G_{\alpha-\beta}^{\text{acc}} + \Delta G_{\alpha-\beta}^{\text{int}}, \quad (4)$$

where $\Delta G_{\alpha-\beta}^{\text{acc}} = W_{\text{acc}}$ is the accommodation energy, and $\Delta G_{\alpha-\beta}^{\text{int}} = W_{\text{int}}$ is the elastic interaction energy. The accommodation energy, $\Delta G_{\alpha-\beta}^{\text{acc}}$, represents the elastic work done on the hydride and the matrix to accommodate the volume dilatation (transformation strain) accompanying the hydride formation from the solid solution in the absence of external stress. It may be calculated from

$$\Delta G_{\alpha-\beta}^{\text{acc}} = -\frac{1}{2} \int_V \sigma_{ij}^I \epsilon_{ij}^T dV, \quad (5)$$

where σ_{ij}^I is the stress in the constrained hydride, ϵ_{ij}^T is the transformation strain in going from a solid solution to the hydride, V is the volume occupied by a mole of hydride (Eshelby, 1956, 1957), and the standard summation convention over the range is implied for a repeated index.

The interaction energy, $\Delta G_{\alpha-\beta}^{\text{int}}$, is due to the energetic interaction of the volume change on hydride formation with an external stress field σ_{ij}^a . It

represents the difference between the potential energy of a system where hydride has formed in the presence of an external stress, and the sum of the potential energy of the hydride-free matrix in the presence of the external stress and the potential energy of the matrix where hydride has formed in the absence of the external stress. In the purely elastic case $\Delta G_{\alpha-\beta}^{\text{int}}$ can be calculated (Eshelby, 1956, 1957) by

$$\Delta G_{\alpha-\beta}^{\text{int}} = - \int_V \sigma_{ij}^a \epsilon_{ij}^T dV, \quad (6)$$

where σ_{ij}^a is the stress due to the applied loads in the absence of the hydride.

For hydride formation with elastoplastic accommodation, (nonlinear material response) (4) is no longer valid. Under these conditions, the following more general formula for the total mechanical energy $\Delta G_{\alpha-\beta}^{\text{mech}}$ is required

$$\Delta G_{\alpha-\beta}^{\text{mech}} = \Delta G_{\alpha-\beta}^e + \Delta G_{\alpha-\beta}^p + \Delta G_{\alpha-\beta}^{\text{ext}}, \quad (7)$$

where $\Delta G_{\alpha-\beta}^e$ is the elastic work done on the system (matrix+hydride) and is stored in the system as elastic energy, $\Delta G_{\alpha-\beta}^p$ is the plastic work dissipation, and $\Delta G_{\alpha-\beta}^{\text{ext}}$ is the work done by the external loads against the matrix displacement upon hydride formation. The change in elastic energy stored in the system, $\Delta G_{\alpha-\beta}^e$, can be evaluated with the use of

$$\Delta G_{\alpha-\beta}^e = \int_V \left(\int_t \sigma_{ij} D_{ij}^e dt \right) dV, \quad (8)$$

where σ_{ij} is the local Cauchy stress, D_{ij}^e is the elastic component of the deformation rate tensor which equals the symmetric part of the velocity gradient in spatial coordinates, t is the time of formation and V now is the volume of the system (matrix+hydride). For a hyperelastic solid, the time integral in equation (8) depends only on the final value of the stress. The plastic work done on the system, $\Delta G_{\alpha-\beta}^p$, can be evaluated with the use of

$$\Delta G_{\alpha-\beta}^p = \int_V \left(\int_t \sigma_{ij} D_{ij}^p dt \right) dV, \quad (9)$$

where D_{ij}^p is the plastic component of the deformation rate tensor and the work done by the external tractions, $\Delta G_{\alpha-\beta}^{\text{ext}}$, can be evaluated with the use of

$$\Delta G_{\alpha-\beta}^{\text{ext}} = \int_S \left(\int_t T_i^{\text{ext}} v_i dt \right) dS \quad (10)$$

where S is the surface bounding the volume V , T_i^{ext} is the component of the applied traction on S , and v_i is the component of the surface velocity. The elasticity based formulation expressed in (4) as $\Delta G_{\alpha-\beta}^{\text{mech}} = \Delta G_{\alpha-\beta}^{\text{acc}} + \Delta G_{\alpha-\beta}^{\text{int}}$ can be viewed as a special case of the more general elastoplastic formulation expressed in (7). Given the inherent path dependency of a plastic deformation accompanying hydride formation, the calculation of the total mechanical energy of formation is model dependent.

Since most metals undergo plastic deformation to allow for the accommodation of hydride (Birnbbaum et al., 1976; Makenas and Birnbbaum, 1980; Puls, 1981, 1984), the terminal solid solubility is not an "equilibrium" value for the solute hydrogen concentration in contact with the hydride phase. The chemical and surface energy terms of (3) represent thermodynamically reversible processes such that $\Delta G_{\alpha-\beta}^{\text{chem}} = -\Delta G_{\beta-\alpha}^{\text{chem}}$ and $\Delta G_{\alpha-\beta}^{\text{sur}} = -\Delta G_{\beta-\alpha}^{\text{sur}}$ (Birnbbaum et al., 1976). However, due to the plastic accommodation of the matrix, a complete cycle of hydride formation and dissolution results in lost energy in the form of thermally dissipated plastic work. Thus in general, $\Delta G_{\alpha-\beta}^{\text{mech}} \neq -\Delta G_{\beta-\alpha}^{\text{mech}}$ and as such $\Delta G_{\alpha-\beta}^{\text{tot}} \neq -\Delta G_{\beta-\alpha}^{\text{tot}}$. Therefore, as suggested by (3), a hysteresis develops and terminal solid solubility or critical hydrogen concentration on formation is not equal to the critical hydrogen concentration on dissolution, i.e., $(c_s^\sigma)_{\alpha-\beta} \neq (c_s^\sigma)_{\beta-\alpha}$.

3. APPLICATION: NIOBIUM SYSTEM

Numerical calculations were carried out to estimate the total mechanical energy of formation of a hydride precipitate with an isotropic linearly elastic response in an infinite niobium matrix and with an isotropic linearly elastic, perfectly plastic response under plane strain conditions. The elastoplastic response of the matrix material requires the hydride precipitation to be modeled in an incremental fashion. In this treatment, it was assumed that the entire volume of the precipitate uniformly acquires the transformation strain that accompanies hydride formation. External forces can be applied so that the entire range of stress space is spanned. The flexibility of the finite element method allowed for ongoing calculations of the change in the stored elastic energy, the plastic work done on the system, and the work done by the external forces.

The precipitating hydride particle and the niobium matrix were modeled as circular cylinders, as seen in Fig. 1. There was no diffusion of hydrogen in this part of the calculation. While it is known that the transformation strain is anisotropic (Somenkov et al., 1968; Rashid and Scott, 1973; Shoher, 1975; Pick and Bausch, 1976), the largest stress contributions to the hydride free energies arise from the dilatational component. Thus in the context of the large strain formulation, the deformation rate due to the hydride is phrased as

$$D_{ij}^T = \frac{d}{dt} \left[\ln \left(1 + \frac{1}{3} e^T \right) \right] \delta_{ij} \quad (11)$$

where d/dt denotes differentiation with respect to time, e^T is the dilatational transformation strain equal to θ_{hyd} which is the volume dilatation of a material element that is 100% hydride and δ_{ij} is the Kronecker delta.

In the case of finite deformations, the associated flow rule for von-Mises yielding and perfect plasticity is given by the classical Prandtl-Reuss equations stated by McMeeking and Rice (1975) and appropriately modified to account for transformation induced strain in the lattice

$$\dot{\sigma}_{ij} = 2G \left[\delta_{ik} \delta_{jl} + \frac{\nu}{1-\nu} \delta_{ij} \delta_{kl} - \frac{3}{2} \frac{\sigma'_{ij} \sigma'_{kl}}{\sigma_0^2} \right] (D_{kl} - D_{kl}^T) \quad (12)$$

for plastic loading and

$$\dot{\sigma}_{ij} = 2G \left(\delta_{ik} \delta_{jl} + \frac{\nu}{1-\nu} \delta_{ij} \delta_{kl} \right) (D_{kl} - D_{kl}^T) \quad (13)$$

for elastic loading or any unloading, where D_{ij} is the deformation rate tensor, the superposed $\dot{}$ denotes the Jaumann or corrotational stress rate which exhibits proper material invariance for rigid spin, $\sigma'_{ij} = \sigma_{ij} - \sigma_{kk} \delta_{ij} / 3$ is the deviatoric stress, σ_0 is the yield stress, G and ν are the shear modulus and Poisson's ratio respectively. Thus the constitutive equation of the elastically deforming hydride cylinder (see Fig. 1) is given by (11) and (13), whereas the constitutive equation of the surrounding elastoplastically deforming niobium cylinder is given by (12) and (13) with D_{ij}^T set equal to zero.

The governing equations for the rate equilibrium accounting for changes of the deformed volume of the material are cited by McMeeking and Rice (1975) as

$$\int_V \left(\dot{\sigma}_{ij} + D_{kk} \sigma_{ij} \right) \delta D_{ij} dV - \int_V \frac{1}{2} \sigma_{ij} \delta \left(2D_{ik} D_{kj} - v_{k,i} v_{k,j} \right) dV = \int_S \dot{T}_i \delta v_i dS \quad (14)$$

where a superposed dot denotes time differentiation, T_i is the traction which is equal to T_i^{ext} on the part of the surface where tractions are prescribed, and δ indicates an arbitrary virtual variation of the quantity it precedes. Note that \dot{T}_i is a nominal rate of change (McMeeking and Rice, 1975). Any virtual variation of the velocity is constrained to vanish on the part of the surface where velocities are prescribed. The finite element equations were derived

from the variational statement (14), and were modified to allow for near incompressible material response (Nagtegaal et al., 1974). The constitutive equations (12) and (13) were integrated by using the backward Euler integration technique (Lufrano, 1996). The formulation of Govindarajan and Aravas (1994) for large strain plasticity was adopted to ensure zero lattice strain during large rigid body rotation.

Young's modulus and Poisson's ratio for the hydride and matrix were 113.65 GPa and 0.39 respectively, the hydride formation volume dilatation was $\theta_{\text{hyd}} = 12\%$, and the yield stress, σ_0 , of niobium was taken to be 400 MPa. At ratios of the radius of the matrix to the radius of the precipitate of greater than 20 to 1, the size effects of the matrix were negligible. Traction $T_i^{\text{ext}} = \Sigma_{ij} n_j$, on the external surface S with outward unit normal n_i were applied all around to control the macroscopic state of stress Σ_{ij} in the composite material (see Fig. 1). The macroscopic stress Σ_{ij} can be described by the macroscopic hydrostatic component

$$\Sigma_m = \frac{1}{3} \Sigma_{kk} \quad (15)$$

and the deviatoric component

$$\Sigma_e = \sqrt{\frac{3}{2} \Sigma'_{ij} \Sigma'_{ij}}, \quad (16)$$

where $\Sigma'_{ij} = \Sigma_{ij} - \Sigma_{kk} \delta_{ij} / 3$. To span the range of possible values of plane strain stress space for a perfectly plastic material it is sufficient to let the normalized macroscopic hydrostatic stress, Σ_m / σ_0 , vary between -4.0 and 4.0 and to let the normalized macroscopic deviatoric stress, Σ_e / σ_0 , vary between zero and one.

3.1. Elastic accommodation

When the accommodation of the hydride is purely elastic, equation (5) yields

$$\Delta G_{\alpha-\beta}^{\text{acc}} = \frac{E(e^T)^2}{9(1-\nu)} V_{\text{hyd}} \quad (17)$$

where e^T , which is equal to θ_{hyd} , is the volume dilatation and $V_{\text{hyd}} = 12.3 \times 10^{-6} \text{ m}^3/\text{mole}$ is the molar volume of the hydride (Hindin and Birnbaum, 1981). Using (17), one can calculate an elastic accommodation energy of $\Delta G_{\alpha-\beta}^{\text{acc}} = 3667$ Joules per mole. Similarly (6) for purely dilatational transformation, results in

$$\Delta G_{\alpha-\beta}^{\text{int}} = -\frac{\sigma_{kk}^a}{3} e^T V_{\text{hyd}}, \quad (18)$$

which in turn provides an interaction energy normalized by the yield stress $\Delta G_{\alpha-\beta}^{\text{int}} = -590.4 \Sigma_m / \sigma_0$ Joules per mole.

For an elastic matrix, the vertical, straight line segments of Fig. 2 represent the total mechanical energy of formation, $\Delta G_{\alpha-\beta}^{\text{mech}} = \Delta G_{\alpha-\beta}^{\text{acc}} + \Delta G_{\alpha-\beta}^{\text{int}}$, per mole of precipitated hydride from the analytic ((17) and (18)) and numerical solutions plotted over the externally applied stress space. The numerical solution was obtained by switching off the yielding of the matrix through use of a sufficiently large value for σ_0 in the finite element calculations. Figure 2 clearly shows that the numerical calculations are in excellent agreement with the analytic solution. The numerical results show a total mechanical energy in the absence of external stress, i.e., the elastic accommodation energy, of 3696 Joules per mole. The numerical results also show a change of the total mechanical energy per unit of normalized macroscopic hydrostatic stress, Σ_m / σ_0 , of 591.7 Joules per mole. Lastly, equations (17) and (18) indicate, and is shown in Fig. 2, that the total mechanical energy, $\Delta G_{\alpha-\beta}^{\text{mech}}$, does not depend on the macroscopic deviatoric stress, Σ_e / σ_0 .

3.2. Elastoplastic accommodation

As previously stated, most metals including niobium undergo plastic deformation to allow for the accommodation of hydride (Birnbaum et al., 1976; Makenas and Birnbaum, 1980; Puls, 1981, 1984). Therefore, of particular interest is how the total mechanical energy of formation changes when the matrix is allowed to plastically deform during hydride precipitation. For an elastic-perfectly plastic matrix, contour plots of the numerical results of the total mechanical energy of formation per mole of precipitated hydride are displayed in Fig. 2 plotted over the externally applied stress space. In this case, the elastoplastic accommodation energy, i.e. $\Delta G_{\alpha-\beta}^{\text{mech}}$ in the absence of external loads, is 2048 Joules per mole. As seen in the Fig. 2, at low levels of deviatoric stress, e.g., $\Sigma_e/\sigma_0 \leq 0.8$, the total mechanical energy exhibits a minimal dependence on the macroscopic deviatoric stress, Σ_e/σ_0 , and the dependence on the macroscopic hydrostatic stress, Σ_m/σ_0 , is approximately linear. For $\Sigma_e/\sigma_0 \leq 0.8$, the change of the total mechanical energy per mole per unit of macroscopic normalized hydrostatic stress, Σ_m/σ_0 , is 595 Joules per mole. However, at a given hydrostatic stress and higher levels of deviatoric stress, e.g., $\Sigma_e/\sigma_0 > 0.8$, the total mechanical energy of formation begins to markedly decrease as the macroscopic deviatoric stress increases, with the largest rate of decrease occurring as the matrix material approaches yield, i.e., $\Sigma_e/\sigma_0 = 1.0$. When hydride precipitates in an elastic-perfectly plastic niobium matrix in the absence of external stress, the numerical results show that equivalent plastic strains of greater than 5 percent develop in the niobium at the boundary with the hydride inclusion. As a result, less energy is required to deform the niobium elastoplastically in order to accommodate the volume change on hydride formation.

3.3. Terminal solid solubility of hydrogen

A stress-free solvus of $c_s^0 = 0.054$ hydrogen atoms per solution atom was calculated by the authors (1996) with use of (1) with $A = 3.74$ and $H_h + W_{acc} = -10.6 \text{ kJ/mole}$ (Puls, 1978; Hindin and Birnbaum, 1981; Sofronis, 1987) at a temperature of 300K. In the elastic-perfectly plastic media, in order for (2) and (3) with $\Delta G_{\alpha-\beta}^{mech} = 2.048 \text{ kJ/mole}$ to yield the same stress-free solvus at the same temperature, one calculates $B = 3.74$ and $\Delta G_{\alpha-\beta}^{chem} + \Delta G_{\alpha-\beta}^{sur} = -12.6 \text{ kJ/mole}$. Now, with these data, (2) and (3), and extrapolated data for $\Delta G_{\alpha-\beta}^{mech}$ from Fig. 2, a calculation of the terminal solid solubility can be made for any level of external stress.

In summary, in the case of elastic accommodation the solvus concentration of hydrogen in solution was calculated by the authors (1996) through

$$c_s^\sigma = 3.74 \exp\left(\frac{-10.6 \text{ kJ/mole}}{RT}\right) \exp\left(\frac{W_{int}}{RT}\right). \quad (19)$$

Equation (18) was used for the calculation of the elastic interaction energy, W_{int} , appropriately modified to account for the inhomogeneity of the stress field, such as near a crack tip (Flanagan et al., 1981) where the hydride and solid solution molar free energies differ in the highly stressed element of volume and the low stressed element of volume. In the present paper, which accounts for the elastoplasticity on hydride formation, the solvus concentration of hydrogen in niobium is calculated through

$$c_s^\sigma = 3.74 \exp\left(\frac{-12.6 \text{ kJ/mole}}{RT}\right) \exp\left(\frac{\Delta G_{\alpha-\beta}^{mech}}{RT}\right), \quad (20)$$

where the total mechanical energy of formation is extrapolated from Fig. 2. A contour plot of the terminal solid solubility c_s^σ , as calculated by (19) and (20), is shown in Fig. 3 plotted over the externally applied stress space. Clearly at a given hydrostatic stress and high levels of deviatoric stress, e.g., $\Sigma_e/\sigma_0 > 0.8$,

the solvus concentration calculated using the elastoplastic formulation is markedly less than the solvus calculated through the elastic formulation.

4. HYDROGEN TRANSPORT AND HYDRIDE FORMATION

Modeling of stress driven transient diffusion of hydrogen and the corresponding formulation of the initial boundary value problem follow the methodology developed by the authors in their previous work (1996). Lufrano and Sofronis (1996) have shown that at 300 K for nominal concentrations around 0.01 hydrogen atoms per solvent atom, hydrogen in niobium resides predominantly in lattice interstitial sites regardless of the level of plastic straining at notches. Thus, in the interest of clarity and economy, this current model ignores hydrogen trapping. The hydrogen diffusion constant was taken to be independent of the local hydrogen concentration and state of stress and the activation energy for hydrogen diffusion through hydride was taken to be equal to three times the activation energy for diffusion through the solid solution phase (Völkl and Alefeld, 1978). Hence, in the present study, the dominant mode for diffusion is through the metal solid solution. To model the conditions representing internal embrittlement, a zero hydrogen flux boundary condition is used.

Formulation of the large strain elastoplastic boundary value problem follows the methodology outlined in Subsection 2.1. The composite material (matrix+hydride) is taken to have an elastoplastic response characterized by (12) and (13) in which the deformation rate tensor, D_{ij}^T , for the volume dilatation due to interstitial hydrogen in solution and hydride formation is given by (11), where e^T is now given by

$$e^T = \begin{cases} (c - c_0)\theta_h & \text{if } f = 0 \\ (1 - f)(c - c_0)\theta_h + f(\theta_{hyd} - c_0\theta_h) & \text{if } f \neq 0 \end{cases} \quad (21)$$

c and c_0 are the local and initial hydrogen concentration in hydrogen atoms per metal atom, respectively, f is the local hydride volume fraction, and θ_h is the lattice local dilatation when a hydrogen atom dissolves in solution with the metal (Peisl, 1978). The yield stress, σ_0 , is assumed to be independent of the local hydrogen concentration and hydride volume fraction.

4.1. *Hydrogen transport and small scale hydride formation at a blunting crack tip*

Modeling was carried out under the assumption of small scale yielding conditions, as seen in Fig. 4 with the initial conditions of a uniform initial concentration, c_0 , hydrogen atoms per niobium atom, below the stress free terminal solid solubility, f , and $\dot{f} = 0$ at $t = 0$. A zero hydrogen flux boundary condition was used. In all of the numerical experiments the crack was loaded under plane strain mode I conditions at a constant displacement rate during a loading time t_l , at the end of which the final load phrased in terms of the applied stress intensity factor was $K_A = 20 \text{ MPa}\sqrt{\text{m}}$. At times greater than t_l the loading displacements were held fixed.

All material parameters were chosen to approximate the niobium-hydrogen system. The molar volume of niobium, V_M , equaled $10.852 \times 10^{-6} \text{ m}^3/\text{mole}$, and the local lattice dilatation, θ_h , on introducing a hydrogen atom in solution with the metal equaled 17.4% (Peisl, 1978). At 300K the diffusion constant of solute hydrogen through the metal, D_s , is equal to $8.3 \times 10^{-10} \text{ m}^2/\text{s}$ (Völkl and Alefeld, 1978). Modeling of hydride formation was carried out using both the elastic, (19), and elastoplastic, (20), methods for determining the terminal solid solubility of hydrogen.

Regardless of the methodology used, at the system's temperature, $T = 300\text{K}$, the terminal solid solubility of hydrogen in solution at zero stress is $c_s^0 = 0.054$ hydrogen atoms per solution atom. As will be shown later, the stress induced formation of hydride results in local stress relaxation raising the possibility of hydride dissolution. In view of the plastic accommodation and resulting hysteresis, dissolution of hydride was not modeled.

4.2. Numerical results

Finite element calculations were carried out with an initial hydrogen concentration $c_0 = 0.02$ hydrogen atoms per metal atom. Figures 5 and 6 show surface plots of the hydride volume fraction, f , plotted in the region in front of a blunted crack (see Fig. 4) after the application of an applied load of $K_A = 20 \text{ MPa}\sqrt{\text{m}}$ in a load time $t_l = 36$ seconds after a total elapsed time, t_e , of 36 and 360 seconds respectively, using the elastic calculation of the terminal solid solubility (19). Figures 5 and 6 clearly illustrate two principle differences in the solution to the hydride formation problem that occur when the material is assumed to have an elastoplastic response as opposed to when the material is treated as elastic, as in the earlier work by the authors (1996). First, in the elastic-perfectly plastic calculations, the hydride volume fraction is never equal to one, hence there is no region in front of the crack that completely transforms into hydride. Secondly, the peak in the local hydride volume fraction occurs approximately 15 microns in front of the crack tip instead of directly at the crack tip. The reasons behind these differences lie in the character of the crack tip stress fields in the two cases. Since tensile hydrostatic stresses lower the value of the solvus, in the singular stress field at the crack tip, (Irwin, 1960), the terminal solid solubility expressed in (19) becomes infinitely small corresponding to the infinite stresses, regardless of

the level of the applied load. However, a blunted crack in an elastic perfectly plastic material produces a maximum mean stress, $\sigma_{kk}/3$, of approximately 3 times the yield stress, σ_0 , at a distance in front of the crack tip of about 2 times the crack opening displacement (McMeeking, 1977). Consequently, the maximum hydride volume fraction occurs well in front of the crack tip. Figures 5 and 6 show that after the loading has been completed the hydride volume fraction continues to increase in the region in front of the crack tip, thus suggesting the autocatalytic hydride growth that has been experimentally observed by Shih et al. (1988).

With the solvus calculated elastically through (19), Fig. 7 shows a surface plot of the hydride volume fraction, f , plotted in the region in front of a blunted crack subjected to an applied load of $K_A = 20 \text{ MPa}\sqrt{\text{m}}$ in a load time $t_l = 360$ seconds at the completion of loading. A comparison of Figs. 6 ($t_l = 36s$ and $t_e = 36s$) and 7 ($t_l = 360s$ and $t_e = 360s$) shows that the amount of hydride formed after a total elapsed time of 360 seconds depends on the loading path for the test specimen with the slow loading resulting in a greater amount of hydride.

With an elastoplastic calculation of the terminal solid solubility (20), Figs. 8 and 9 show surface plots of the hydride volume fraction, f , plotted in the region in front of a blunted crack subjected to an applied load of $K_A = 20 \text{ MPa}\sqrt{\text{m}}$ in a load time $t_l = 36$ seconds, after the completion of loading ($t_e = 36s$) and after a total elapsed time $t_e = 360$ seconds, respectively. These data show continued hydride growth after the loading has been completed. Figure 10 shows a surface plot of the hydride volume fraction, f , plotted in the region in front of a blunted crack subjected to an applied load of $K_A = 20 \text{ MPa}\sqrt{\text{m}}$ in a load time $t_l = 360$ seconds at the completion of loading ($t_e = 360s$) using the elastoplastic calculation of the terminal solid solubility. Again a

dependence of the amount of the hydride on the loading path is shown. As mentioned earlier, as the tensile hydrostatic stresses develop in the region in front of the crack tip, the formation of hydride is energetically more favorable, although, the stress fields are not the sole determining factor for hydride formation. Even though the current model does not examine the kinetics of the formation of actual hydride particles, the necessity of time to allow interstitial hydrogen to diffuse to the crack tip gives the hydride formation problem a sensitivity to the loading rate as well as the actual level of load.

A comparison of Figs. 5–10 shows that consideration of the elastoplastic energy of formation leads to a prediction of larger hydride volume fractions over a larger region ahead of the blunted crack. The principle reason for this stems from the decrease in the elastoplastic energy of formation that, as illustrated in Fig. 3, occurs as the deviatoric stresses in the niobium matrix nears the yield stress. Therefore, as the niobium begins to deform plastically during the loading of the crack, the formation of hydride becomes energetically more favorable. In addition to the prediction of a larger hydride zone size in the results using the elastoplastic calculation of the solvus, also of note is that the hydride zone has a definite nonzero component that extends obliquely from the crack tip. This is a direct result of the effect of the deviatoric stresses near yield on the elastoplastic energy of formation, which specifically results in a significant lowering of the energy of formation and hence a lowering of the solvus concentration. The oblique hydride growth can be better visualized in Fig. 11, which shows contour plots of the hydride volume fraction, f , in the area in front of a blunted crack subjected to an applied load of $K_A=20 \text{ MPa}\sqrt{\text{m}}$ in loading time of $t_l=360$ seconds after the completion of loading ($t_e=360\text{s}$). Thus, even with a continuum model, which ignores the effects of crystalline slip planes, the numerical results

suggest the possibility of "three-pronged" hydride growth in front of a crack, a result observed in α -Ti-4 wt%Al by Shih et al., (1988). In view of the probabilistic approach to hydride formation, one may infer from these results the possibility of hydride growth along lines oblique to the crack, as well as along lines directly in front of and parallel to the crack. It should be noted that these results are a direct consequence of the consideration of elastoplastic energy of hydride formation and accordingly they are not predicted under the assumption of entirely elastic accommodation of the hydride formation. These results are also consistent with the observations that hydrides form along slip lines in front of a stressed notch (Grossbeck and Birnbaum, 1977).

With an elastoplastic calculation for the terminal solid solubility (20), Fig. 12 shows the hydride volume fraction, f , in front of the blunting crack tip subjected to an applied load of $K_A = 20 \text{ MPa}\sqrt{\text{m}}$ in load times of $t_l = 36$ and 360 seconds plotted against the distance from the crack tip, R , at $\theta = 0$, for total elapsed times of 36 and 360 seconds. In addition, Fig. 12 shows hydride growth after the completion of loading. The hydride volume fraction profile of Fig. 12 was found to be significantly higher and broader than the profile calculated using the elastic formulation of the solvus concentration, despite the qualitative similarity of the results in the two cases. Figure 12 clearly shows that the development of the hydride depends on the loading strain rate and the loading path in addition to the load level. One of the reasons for the path dependence and hence, the different hydride volume fraction profile after an elapsed time of 360 seconds, will become clearer upon examination of the effect of hydride formation on the state of stress in front of the crack tip.

5. HYDRIDE INDUCED STRESS RELAXATION AND ENHANCED PLASTICITY AT A CRACK TIP

In the absence of hydride formation, Lufrano and Sofronis (1996) have found that there is only a mild elevation, less than 2 times the initial concentration of 0.01 hydrogen atoms per niobium atom, of the local hydrogen concentration ahead of a notch or a crack tip due to the local hydrostatic stress effect. As a result, the relaxation caused by the hydrogen induced dilatational strain, which is less than 0.35%, is of minor importance and does not affect the local stresses at initial concentrations of the order of 0.01. However, when hydride forms in niobium, the volume dilatation is approximately 12 percent (Puls, 1981, 1984) and it is expected that the corresponding stress relaxation will become more significant.

Figures 13 and 14, using the elastic, (19), and elastoplastic, (20), calculations of the terminal solid solubility, respectively, and a nominal hydrogen concentration of 0.02 H/M, show the normalized normal stress, σ_{22}/σ_0 , in front of a blunted crack tip subjected to an applied load of $K_A=20 \text{ MPa}\sqrt{\text{m}}$ in load times of $t_l=36$ and 360 seconds plotted against the distance from the crack tip, R , at $\theta=0$, for total elapsed times of 36 and 360 seconds. For reference purposes the normalized normal stress, σ_{22}/σ_0 , from a hydrogen-free sample is also plotted in the figures. Figures 13 and 14 clearly illustrate that reductions in the normal stress in front of the crack occur due to the formation of hydride for both the elastic and elastoplastic formulation of the solvus concentration. Both the development of the hydride and the amount of stress relaxation that occurs are dependent on the loading strain rate. The model that uses the elastic calculation of the terminal solid solubility predicts less hydride formation than the elastoplastic and hence a

smaller stress reduction is calculated for the elastic accommodation. The small oscillations in the stress field displayed in Fig. 14 are a numerical by-product of the solution to the highly sensitive nonlinear coupled equations using the elastoplastic calculation of the solvus concentration.

Figures 13 and 14 show that continued stress relaxation occurs in conjunction with the postloading autocatalytic hydride growth. For the calculations using the elastic and elastoplastic formulations of the solvus concentration, a respective 16 and 23 percent reduction in the peak normal stress in front of the crack tip occurs after a total elapsed time of 360 seconds.

While the formation of hydride has been shown to reduce the stresses in front of the crack tip, it is reasonable to question the effect of the dilatational strain induced by the hydride precipitation on the levels of strain. Figure 15 shows the equivalent plastic strain, ϵ^p , in front of a blunted crack tip subjected to an applied load of $K_A = 20 \text{ MPa}\sqrt{\text{m}}$ in loading times of $t_l = 36$ and 360 seconds plotted against the distance from the crack tip, R , at $\theta = 0$, for total elapsed times of 36 and 360 seconds, using the elastoplastic calculation of the terminal solid solubility and a nominal hydrogen concentration of 0.02 H/M. For reference purposes the equivalent plastic strain, ϵ^p , from a hydrogen-free sample is also plotted in the figure. Figure 15 shows that the formation of hydride causes as much as a 140 percent increase in the plastic strain at a distance of 10 microns in front of the crack tip in comparison to a hydrogen-free specimen. As with the formation of hydride and the reduction of stresses, the level of plastic strain depends on the loading path. Thus, the final state of stress, strain, and hydride volume fraction near a crack tip depends on the history of the system as well as the absolute level of the load.

Before closing the examination of the stress relaxation, which results from the formation of hydride, it is informative to study the mode I opening

of a blunted crack tip in niobium under different test conditions. In all of the calculations up to this point, a nominal hydrogen concentration $c_0=0.02$ hydrogen atoms per metal atom and a temperature of 300 K have been used. If the temperature is raised to 500 K, the formation of hydride is no longer energetically favorable, even at hydrogen concentrations as high as 0.8 hydrogen atoms per metal atom (Gahr and Birnbaum, 1978). At $T = 500$ K the diffusion constant of hydrogen through the lattice is $D_s=4.3 \times 10^{-9} \text{ m}^2/\text{s}$ (Völkl and Alefeld, 1978). With a nominal hydrogen concentration $c_0=0.3$ hydrogen atoms per metal atom, Fig. 16 shows the normalized hydrogen concentration, c/c_0 , in front of a crack subjected to an applied load of $K_A=20 \text{ MPa}\sqrt{\text{m}}$ for loading times of $t_l=36, 360$, and 3600 seconds plotted against the distance from the crack tip, R , at the completion of loading. In this calculation the formation of hydride is not modeled and the diffusion constant of the solute hydrogen is taken to be independent of the hydrogen concentration even though the solute hydrogen can no longer be considered dilute. Because the diffusion of hydrogen is so much faster at 500 K than at 300 K, the level of solute hydrogen in equilibrium with the local stress fields is reached in a relatively short time.

Under the same conditions, Fig. 17 shows the normalized normal stress, σ_{22}/σ_0 , in front of a crack tip at the completion of loading in times of $t_l=36, 360$, and 3600 seconds plotted against the distance from the crack tip, R . For reference purposes the normalized normal stress, σ_{22}/σ_0 , from a hydrogen-free sample is also displayed. In this example, with the relatively high nominal hydrogen concentration, the stress-induced enhancement in the local hydrogen concentration are large enough to cause stress relaxation in front of the crack tip. Therefore, it may be concluded that the uncoupling of the hydrogen diffusion and elastoplastic deformation problems is only

possible when the nominal hydrogen concentration is small (~ 0.01 H/M), (Lufrano and Sofronis, 1996), and hydride formation does not occur.

6. IMPLICATIONS FOR HYDRIDE INDUCED CRACK INITIATION

Brittle fracture of the hydride phase, crack advance, and subsequent failure has been experimentally observed (Gahr et al., 1980; Birnbaum, 1984; Shih et al., 1988). Cleavage of a hydride particle in front of the crack tip may be modeled by using a Griffith approach to the fracture event. A necessary relationship can be obtained between the length, a , of the hydride particle, the energy needed to create new surface in the hydride, and the normal stress, σ_{22} , in order for the cleavage event to be energetically favorable. For the formation of a penny shaped crack, the expression for the stress is given by

$$\sigma_{22} = \left[\frac{2\gamma_s E}{\pi(1-\nu^2)a} \right]^{1/2} \quad (22)$$

where γ_s is the surface energy of the hydride phase taken for niobium to be 5.04 Joules/m^2 (Gahr et al., 1980).

Since the transient stress field, σ_{22} , in front of a crack can be monitored at any time during or after the loading of the test sample, a value for the critical size, i.e. length, of a hydride particle for cleavage to occur can be calculated with

$$a_{\text{crit}} = \frac{2\gamma_s E}{\pi(1-\nu^2)\sigma_{22}^2} \quad (23)$$

Using the values of stress from the sample loaded in 36 seconds, displayed in Fig. 14, one can plot the critical hydride particle size, a_{crit} , in front of a crack tip at applied load of $K_A = 20 \text{ MPa}\sqrt{\text{m}}$ against the distance from the crack tip, R , at $\theta = 0$, after the completion of loading, as in Fig. 18. Figure 18 shows that

if a hydride particle forms in the region from 10 to 100 microns in front of the crack tip and is over 0.5 microns in length, then the brittle fracture of that particle is energetically favorable. Once the hydride particle cleaves, either the main crack advances through the cleaved hydride or new hydride is formed at the new stress concentration regions around the cleaved hydride particle. The newly formed hydride may subsequently cleave, setting off a continuing process, which may end in the failure of the specimen.

One shortcoming, however, of the probabilistic modeling of hydride formation is that it does not deliver any information on the size of the hydride particles. Thus, in lieu of experimental data on hydride particle size or a model to monitor the kinetics of individual hydride particle growth in front of the crack tip, a method is needed to estimate the hydride particle size. In the following, a heuristic argument will be used for the estimation of the hydride size and in turn for the estimation of the fracture resistance of the material. The argument is ad-hoc, but it definitely shows how the methodology and results of the present paper can be used to obtain a conservative assessment of the fracture toughness of the material.

Suppose that the region directly in front of the crack tip with a hydride volume fraction $f = f_0 = 0.5$ is 10 microns in length. Then it might be reasonable to assume that an individual hydride particle in this region could be as large as 5 microns in length. With this method of estimation of the hydride particle size, it is possible to monitor the hydride growth in front of the crack (see Fig. 12) and to predict at what time and load a hydride particle size, a , might reach the critical hydride size, as expressed by (23). By varying the above scheme for the estimation of the length of a hydride particle in the region in front of the crack tip, one may obtain a somewhat more conservative fracture criterion. For example, the length of the hydride

particle might be assumed to be equal to the length of the region in front of the crack tip with hydride fraction $f_0 = 0.3$ or $f_0 = 0.1$ multiplied by a factor of 0.3 or 0.1, respectively. In the numerical experiments, the level of the applied load is incrementally applied in a linear fashion until the fracture criterion is reached. Therefore, one may define the fracture toughness in the presence of hydrogen, K_{IC} , as the level of the applied load measured in terms of applied stress intensity factor, K_A , at the point when the fracture criterion, $a = a_{crit}$, is satisfied. This is a conservative fracture toughness prediction since the presence of a void ahead of a blunting crack tip due to cracking of a hydride particle does not necessarily lead to fracture.

Figure 19 shows the level of the applied stress intensity factor, K_{IC} , when the fracture criterion listed above was satisfied, for a test sample loaded at rates of 0.56, 0.056, and 0.0056 MPa \sqrt{m}/s . The fracture toughness, K_{IC} , is sensitive to the loading rate and to the size of the hydride plate which is proportional to f_0 (Fig. 19). As the loading rate increases, since the ability of diffusion to deliver hydrogen to the crack tip, thereby allowing the formation of hydride, is independent of stress, the amount of plasticity which precedes formation of the critical hydride size increases and hence the fracture toughness, K_{IC} , increases. For the fracture criterion that uses the length of material in which $f = f_0 = 0.5$ to determine the hydride particle size, the fracture criterion is not satisfied at a loading rate of 0.56 MPa \sqrt{m}/s when the loading is completed at a level of $K_A = 20$ MPa \sqrt{m} , since at that loading rate the peak hydride volume fraction is just $f = 0.5$. Naturally, the fracture toughness, K_{IC} , of niobium in the presence of hydrogen, as defined above, will also depend on such variables as the temperature and the nominal hydrogen concentration.

7. CLOSURE

An example of hydride formation at a blunting crack tip under plane strain tensile loading in niobium has been presented. The model assumes both elastic and elastoplastic accommodation of the forming hydride and is based on a purely dilatant transformation strain upon precipitation. To this end, a separate model has been developed to calculate the terminal solid solubility of hydrogen in an elastoplastic matrix. The probabilistic formation of hydrides has been modeled using the elastic and elastoplastic calculation for the solvus concentration. For the model using the elastoplastic calculation for the solvus concentration, hydride precipitation has been predicted along lines obliquely aligned to the line of the crack as well as along a line directly in front of the crack. The elastoplastic calculation for the solvus concentration leads to a prediction of a larger hydride zone in comparison to the prediction using the standard elastic accommodation arguments. Under a fixed temperature and nominal concentration of hydrogen the profile of the hydride volume fraction is strongly dependent on the applied load and loading rate. The results suggest autocatalytic hydride growth after the completion of loading. The formation of hydride induces stress relaxation and plastic strain enhancement in the region in front of the crack tip. Hydrogen induced stress relaxation at the crack tip has also been demonstrated at high nominal hydrogen concentrations and at temperatures for which the formation of hydride is not energetically favorable. A fracture criterion based on a Griffith approach for the brittle fracture of hydride particles has been proposed. The fracture criterion suggests that the fracture toughness of the hydride forming material in the presence of hydrogen is dependent on the loading strain rate.

ACKNOWLEDGEMENT

This work was supported by the Department of Energy under grant DEFGO2-91ER45439.

REFERENCES

- Birnbaum, H. K., Grossbeck M. L. and Amano M. (1976) Hydride precipitation in Nb and some properties of NbH. *J. Less Comm. Met.* **49**, 357-370.
- Birnbaum, H. K. (1984) Hydrogen related second phase embrittlement of solids. *Hydrogen Embrittlement and Stress Corrosion Cracking* (Proceedings of a Troiano Festschrift Symposium, Case Western Reserve University, June 1-3, 1980) (ed. by R. Gibala and R. F. Hehemann), pp. 153-177. ASM, OH.
- Birnbaum, H. K. (1990) Mechanisms of hydrogen related fracture of metals. *Hydrogen Effects on Material behavior* (Proceedings of the Fourth International Conference on the Effect of Hydrogen on the Behavior of Materials, Moran, Wyoming, September 12-15, 1989) (ed. by N. R. Moody and A. W. Thompson), pp. 639-690. The Minerals Metals and Materials Society, Warrendale, PA.
- Earmme, Y. Y., Johnson, W. C. and Lee J. K. (1981) Plastic relaxation of the transformation strain energy of a misfitting spherical precipitate: linear and power law strain hardening. *Met Trans.* **12A**, 1521-1529.
- Eshelby, J. D. (1956) The continuum theory of lattice defects. *Solid State Physics* (ed. F. Seitz and D. Turnbull), Vol. 3, pp. 79-144. Academic Press, New York.

- Eshelby, J. D. (1957) The determination of the elastic field of an ellipsoidal inclusion and related problems. *Proc. R. Soc.* **A241**, 376-396.
- Flanagan, T. B., Mason, N. B. and Birnbaum, H. K. (1981) The effect of stress on hydride precipitation. *Scr. Met.* **15**, 109-112.
- Gahr, S. and Birnbaum, H. K., (1978) Hydrogen embrittlement of Nb III - High temperature behavior. *Acta Metall.* **26**, 1781-1788.
- Gahr, S., Grossbeck, M. L. and Birnbaum, H. K., (1977) Hydrogen embrittlement of Nb I - Macroscopic behavior at low temperatures. *Acta Metall.* **25**, 125-134.
- Gahr, S., Makenas, B. J. and Birnbaum, H. K., (1980) Fracture of niobium hydrides. *Acta Metall.* **28**, 1207-1213.
- Govindarajan, R. M. and Aravas, N. (1994) Deformation processing of metal powders: part I - Cold isostatic pressing. *Int. J. Mech. Sci.* **36**, 343-357.
- Grossbeck, M. L. and Birnbaum, H. K., (1977) Low temperature hydrogen embrittlement of niobium II - Microscopic observations. *Acta Metall.* **25**, 135-147.
- Hindin, B. S. and Birnbaum, H. K. (1981) Fracture kinetics of hydrogen embrittled niobium. Technical Report-Office of Naval Research (USN 00014-75-C-1012), University of Illinois at Urbana-Champaign.
- Irwin, G. R. (1960) Fracture mechanics. Structural Mechanics (Proceedings of the First Symposium of Naval Structural Mechanics) (ed. by J. N. Goodier and N. J. Hoff), pp. 557-594. Stanford University, August 1958.
- Lee, J. K., Earmme, Y. Y., Aaronson, H. I. and Russell, K. C. (1980) Plastic relaxation of the transformation strain energy of a misfitting spherical precipitate: ideal plastic behavior. *Met Trans.* **11A**, 1837-1874.

- Leitch, B. W. and Puls M. P. (1992) Finite element calculations of the accommodation energy of a misfitting precipitate in an elastic-plastic matrix. *Met Trans.* **23A**, 797-806.
- Lufrano, J. M. (1996) Hydrogen transport in ydride and non-hydride forming metals and the mechanistic implications for fracture behavior. Ph.D. Thesis, University of Illinois at Urbana-Champaign, Urbana, IL.
- Lufrano, J. M. and Sofronis, P. (1996) Enhanced hydrogen concentrations ahead of rounded notches and cracks - competition between plastic strain and hydrostatic stress. *Met. Trans.* Submitted for publication.
- Lufrano, J. M., Sofronis, P. and Birnbaum, H. K. (1996) Modeling of hydrogen transport and elastically accommodated hydride formation near a crack tip. *J. Mech. Phys. Solids* **44**, 179-205.
- Makenas, B. J. and Birnbaum, H. K. (1980) Phase changes in the niobium-hydrogen system I: Accommodation effects during hydride precipitation. *Acta Metall.* **28**, 979-988.
- McMeeking, R. M. (1977) Finite deformation analysis of crack-tip opening in elastic-plastic materials and implications for fracture. *J. Mech. Phys. Solids* **25**, 357-381.
- McMeeking, R. M. and Rice, J. R. (1975) Finite-element formulations for problems of large elastic-plastic deformation. *Int. J. Solids Structures* **11**, 601-616.
- Nagtegaal, J. C., Parks, D. M. and Rice, J. R. (1974) On numerically accurate finite element solutions in the fully plastic range. *Comp. Meth. Appl. Mech. Eng.* **4**, 153-177.
- Pardee, W. J. and Paton, N. E. (1980) Model of sustained load cracking by hydride growth in Ti alloys. *Met. Trans.* **11A**, 1391-1400.

- Peisl, H. (1978) Lattice strains due to hydrogen in metals. *Hydrogen in Metals I, Topics in Applied Physics* (ed. G. Alefeld and J. Volkl), Vol. 28, pp. 53-74. Springer-Verlag, New York.
- Pick, M. M. and Bausch, R. (1976) The determination of the force-dipole tensor of hydrogen in niobium. *J. Phys. F: Metal Phys.* **6**, 1751-1763.
- Puls, M. P. (1978) Hydrogen induced delayed cracking: 1. strain energy effects on hydrogen solubility. Atomic Energy of Canada Limited Report, AECL-6302, Pinawa, Manitoba.
- Puls, M. P. (1981) The effects of misfit and external stresses on the terminal solid solubility in hydride-forming metals. *Acta Metall.* **29**, 1961-1968.
- Puls, M. P. (1984) Elastic and plastic accommodation effects on metal-hydride solubility. *Acta Metall.* **32**, 1259-1269.
- Rashid, M. S. and Scott, T. E. (1973) Crystal structure of niobium hydrides. *J. Less Comm. Met.* **30**, 399-403.
- Schober, T. (1975) The niobium-hydrogen system--an electron microscope study. *Phys. Stat. Soli.* **30**, 107-116.
- Sen, S. and Balasubramanian, R. (1996) Finite element evaluation of elastoplastic accommodation energies during solid state transformations: coherent, spherical precipitate in finite matrix. *Acta Metall.* To appear.
- Shih, D. S., Robertson, I. M. and Birnbaum, H. K. (1988) Hydrogen embrittlement of α titanium: in situ TEM studies. *Acta Metall.* **36**, 111-124.
- Simpson, L. A. and Puls, M. P. (1979) The effects of stress, temperature and hydrogen content on hydride-induced crack growth in Zr-2.5%Nb. *Met. Trans.* **10A**, 1093-1105.

- Somenkov, V. A., Gurskaya, A. V., Zemlyanov, M. G., Kost, M. E, Chernoplekov, N. A, Chertkov, A. A. (1968) Neutron scattering study of structure and phase transitions in niobium hydrides and deuterides. *Soviet Physics - Solid State*, **10**, 1076-1082.
- Sofronis, P. (1987) Mechanics of hydrogen embrittlement. Ph.D. Thesis, University of Illinois at Urbana-Champaign, Urbana, IL.
- Völkl, J. and Alefeld, G. (1978) Diffusion of hydrogen in metals. *Hydrogen in Metals I, Topics in Applied Physics* (ed. G. Alefeld and J. Volkl), Vol. 28, pp. 53-74. Springer-Verlag, New York.
- Westlake, D. G. (1969) A generalized model for hydrogen embrittlement. *Trans. ASM* **62**, 1000-1006.

FIGURE CAPTIONS

- Fig. 1. The system in plane strain deformation and a representation for the contour plots of the total mechanical energy of hydride formation, $\Delta G_{\alpha-\beta}^{\text{mech}}$, in stress space (elastoplastic matrix response).
- Fig. 2. The total mechanical energy of hydride formation, $\Delta G_{\alpha-\beta}^{\text{mech}}$, in stress space shown in an elastic matrix by vertical straight line segments for the analytic (—) and numerical (- -) solutions, and in an elastic-perfectly plastic matrix by the contour plots .
- Fig. 3. Contour plots in stress space of the solvus concentration, c_s^σ , hydrogen atoms per solute atom, calculated elastically (- -) through (19) and elastoplastically (—) through (20).
- Fig. 4. Description of the boundary and initial conditions for the coupled diffusion and elastoplastic boundary value problems at a blunting crack tip in niobium under small scale yielding and hydride precipitation

conditions. Constant c_0 is the initial concentration, b_0 is the crack opening displacement in the undeformed state, L is the distance from the crack tip equal to $30000b_0$, n_i is the outward unit normal to the external boundary, v_i is the displacement, K_I is the mode I applied stress intensity factor, T_i is the traction, and j_i is the hydrogen flux.

Fig. 5. Surface plot of the hydride volume fraction, f , in the region in front of a blunted crack after the completion of loading, ($K_I = K_A = 20 \text{ MPa}\sqrt{m}$). The load time was $t_l = 36$ seconds and solvus was calculated using the elastic formulation (19). The initial concentration c_0 was 0.02 hydrogen atoms per niobium atom and the temperature 300 K.

Fig. 6. Surface plot of the hydride volume fraction, f , in the region in front of a blunted crack after an elapsed time of 360 seconds. The load time was $t_l = 36$ seconds, $K_I = K_A = 20 \text{ MPa}\sqrt{m}$, and the solvus was calculated using the elastic formulation (19). The initial concentration c_0 was 0.02 hydrogen atoms per niobium atom and the temperature 300 K.

Fig. 7. Surface plot of the hydride volume fraction, f , in the region in front of a blunted crack after the completion of loading ($K_I = K_A = 20 \text{ MPa}\sqrt{m}$). The load time was $t_l = 360$ seconds and the solvus was calculated using the elastic formulation (19). The initial concentration c_0 was 0.02 hydrogen atoms per niobium atom and the temperature 300 K.

Fig. 8. Surface plot of the hydride volume fraction, f , in the region in front of a blunted crack after the completion of loading, ($K_I = K_A = 20 \text{ MPa}\sqrt{m}$). The load time was $t_l = 36$ seconds and solvus was calculated using the elastoplastic formulation (20). The initial concentration c_0 was 0.02 hydrogen atoms per niobium atom and the temperature 300 K.

Fig. 9. Surface plot of the hydride volume fraction, f , in the region in front of a blunted crack after an elapsed time of 360 seconds. The load time was

$t_l=36$ seconds, $K_I = K_A = 20 \text{ MPa}\sqrt{m}$ and the solvus was calculated using the elastoplastic formulation (20). The initial concentration c_0 was 0.02 hydrogen atoms per niobium atom and the temperature 300 K.

Fig. 10. Surface plot of the hydride volume fraction, f , in the region in front of a blunted crack after the completion of loading, ($K_I = K_A = 20 \text{ MPa}\sqrt{m}$). The load time was $t_l=360$ seconds and the solvus was calculated using the elastoplastic formulation (20). The initial concentration c_0 was 0.02 hydrogen atoms per niobium atom and the temperature 300 K.

Fig. 11. Contour plot of the hydride volume fraction, f , in the region in front of a blunted crack after the completion of loading, ($K_I = K_A = 20 \text{ MPa}\sqrt{m}$). The load time was $t_l=360$ seconds and solvus was calculated using the elastoplastic formulation (20). The initial concentration c_0 was 0.02 hydrogen atoms per niobium atom and the temperature 300 K.

Fig. 12. Plot of the hydride volume fraction, f , versus distance, R , ahead of the crack tip at $\theta=0$ after total elapsed times $t_e=36$ and 360 seconds. The load times were $t_l=36$ and 360 seconds, $K_I = K_A = 20 \text{ MPa}\sqrt{m}$, and solvus was calculated using the elastoplastic formulation (20). The initial concentration c_0 was 0.02 hydrogen atoms per niobium atom and the temperature 300 K.

Fig. 13. Plot of the normalized normal stress, σ_{22}/σ_0 , versus distance, R , ahead of the crack tip at $\theta=0$ after total elapsed times $t_e=36$ and 360 seconds. The load times were $t_l=36$ and 360 seconds, $K_I = K_A = 20 \text{ MPa}\sqrt{m}$, and solvus was calculated using the elastic formulation (19). The initial concentration c_0 was 0.02 hydrogen atoms per niobium atom and the temperature 300 K.

Fig. 14. Plot of the normalized normal stress, σ_{22}/σ_0 , versus distance, R , ahead of the crack tip at $\theta=0$ after total elapsed times $t_e=36$ and 360 seconds. The load times were $t_l=36$ and 360 seconds, $K_I = K_A = 20 \text{ MPa}\sqrt{m}$, and solvus was calculated using the elastoplastic formulation (20). The initial concentration c_0 was 0.02 hydrogen atoms per niobium atom and the temperature 300 K.

Fig. 15. Plot of the equivalent plastic strain, ϵ^p , versus distance, R , ahead of the crack tip at $\theta=0$ after total elapsed times $t_e=36$ and 360 seconds. The load times were $t_l=36$ and 360 seconds, $K_I = K_A = 20 \text{ MPa}\sqrt{m}$, and the solvus was calculated using the elastoplastic formulation (20). The initial concentration c_0 was 0.02 hydrogen atoms per niobium atom and the temperature 300 K.

Fig. 16. Plot of the normalized hydrogen concentration, c/c_0 , versus distance, R , ahead of the crack tip at $\theta=0$ after the completion of loading ($K_I = K_A = 20 \text{ MPa}\sqrt{m}$) for load times of $t_l=30, 300$, and 3000 seconds. The initial concentration c_0 was 0.3 hydrogen atoms per niobium atom and the temperature 500 K.

Fig. 17. Plot of the normalized normal stress, σ_{22}/σ_0 , versus distance, R , ahead of the crack tip at $\theta=0$ after the completion of loading ($K_I = K_A = 20 \text{ MPa}\sqrt{m}$) for load times of $t_l=30, 300$, and 3000 seconds. The initial concentration was 0.3 hydrogen atoms per niobium atom and the temperature 500 K.

Fig. 18. Plot of the critical hydride particle size, a_{crit} , versus distance, R , ahead of the crack tip at $\theta=0$ after the completion of loading ($K_I = K_A = 20 \text{ MPa}\sqrt{m}$) at time $t_l=36$ seconds. The terminal solid solubility was calculated with the elastoplastic formulation (20). The

initial concentration c_0 was 0.02 hydrogen atoms per niobium atom and the temperature 300 K.

Fig. 19. Plot of the predicted fracture toughness, K_{IC} , versus the loading rate for three different estimations of the hydride particle size. The elastoplastic formulation (20) was used for the calculation of the solvus. The initial concentration c_0 was 0.02 hydrogen atoms per niobium atom, and the temperature 300 K.

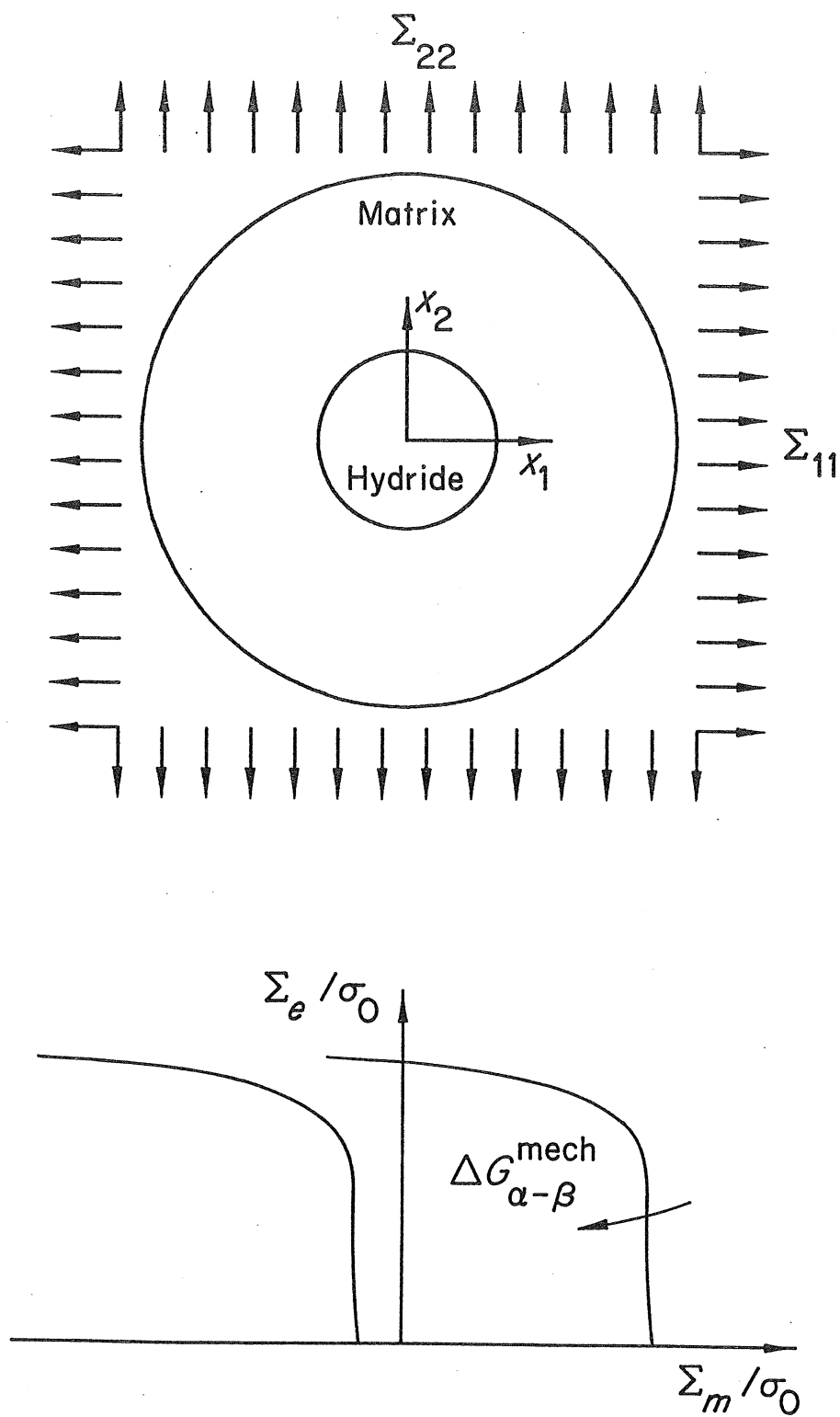


Fig. 1

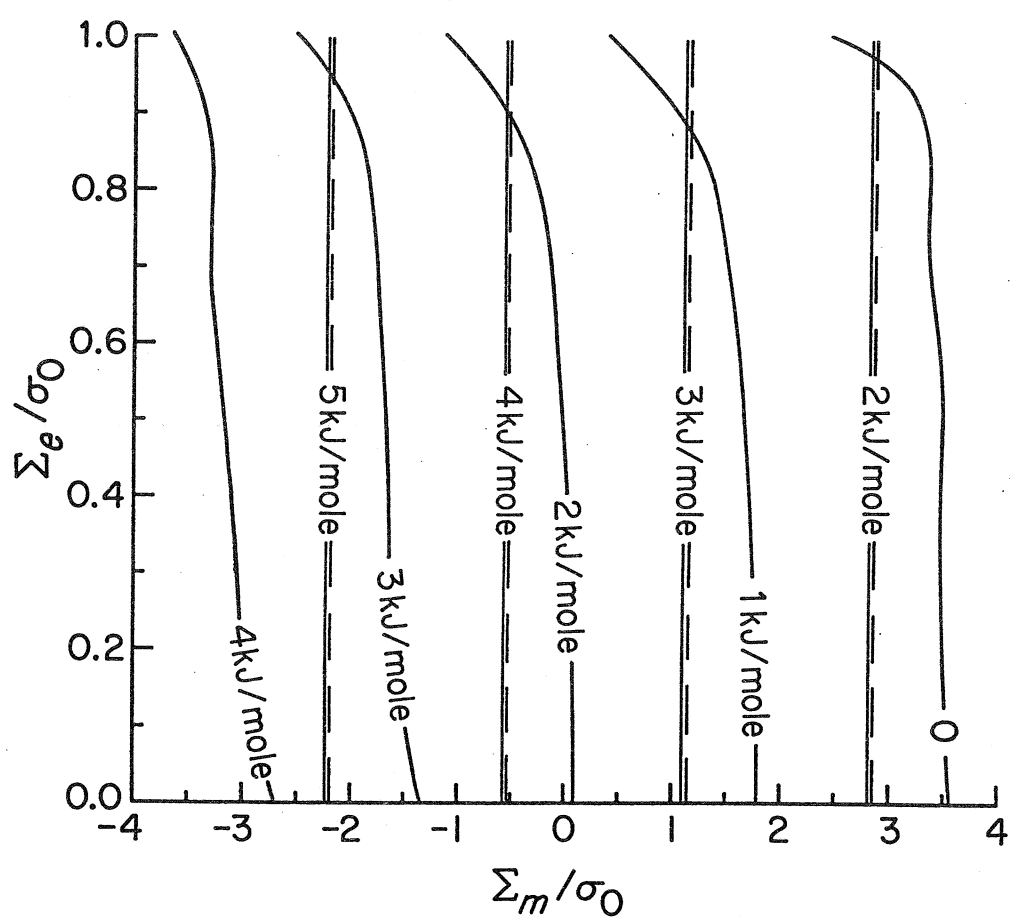


Fig. 2

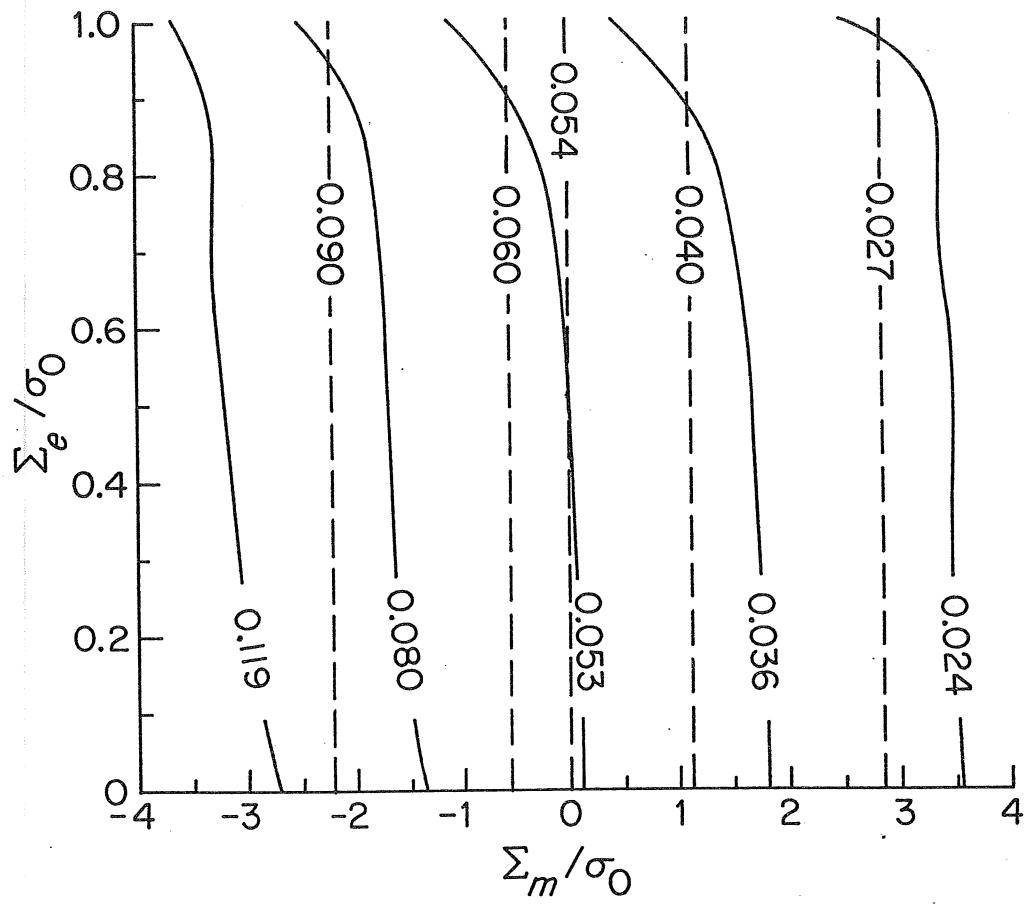


Fig. 3

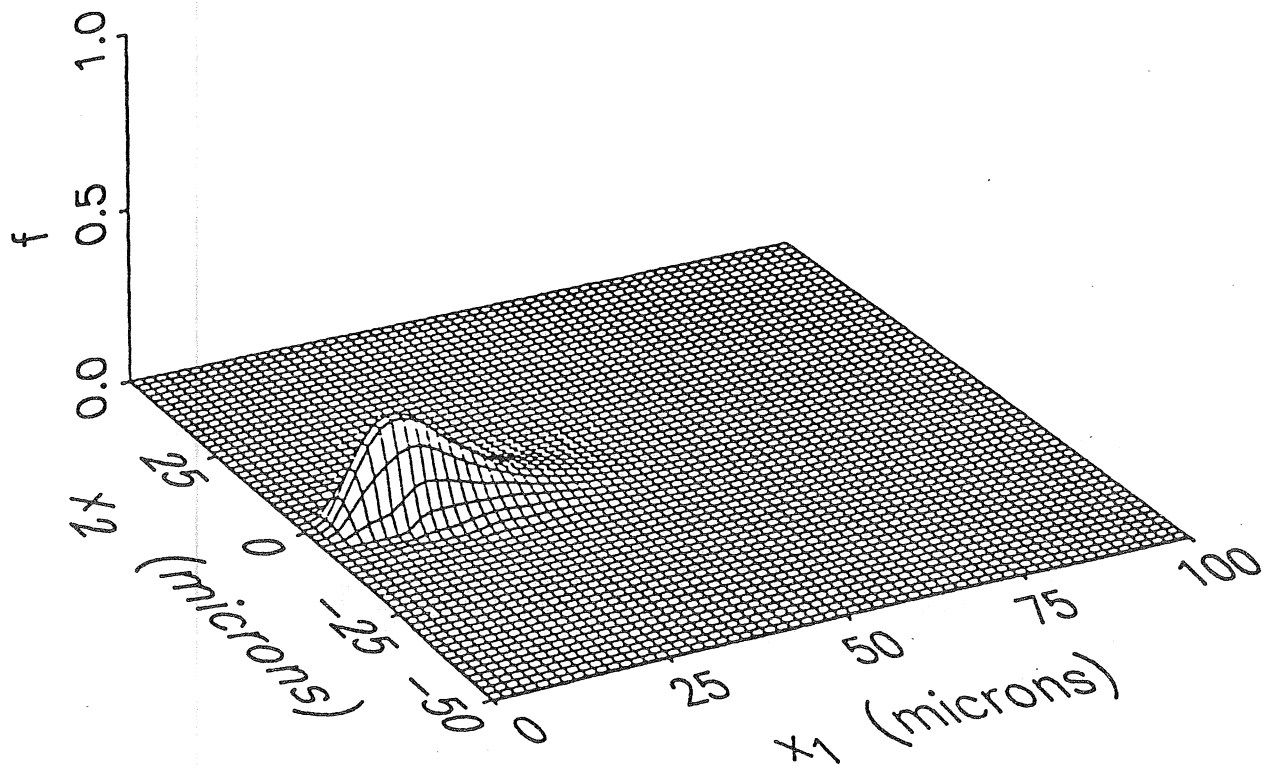


Fig. 5

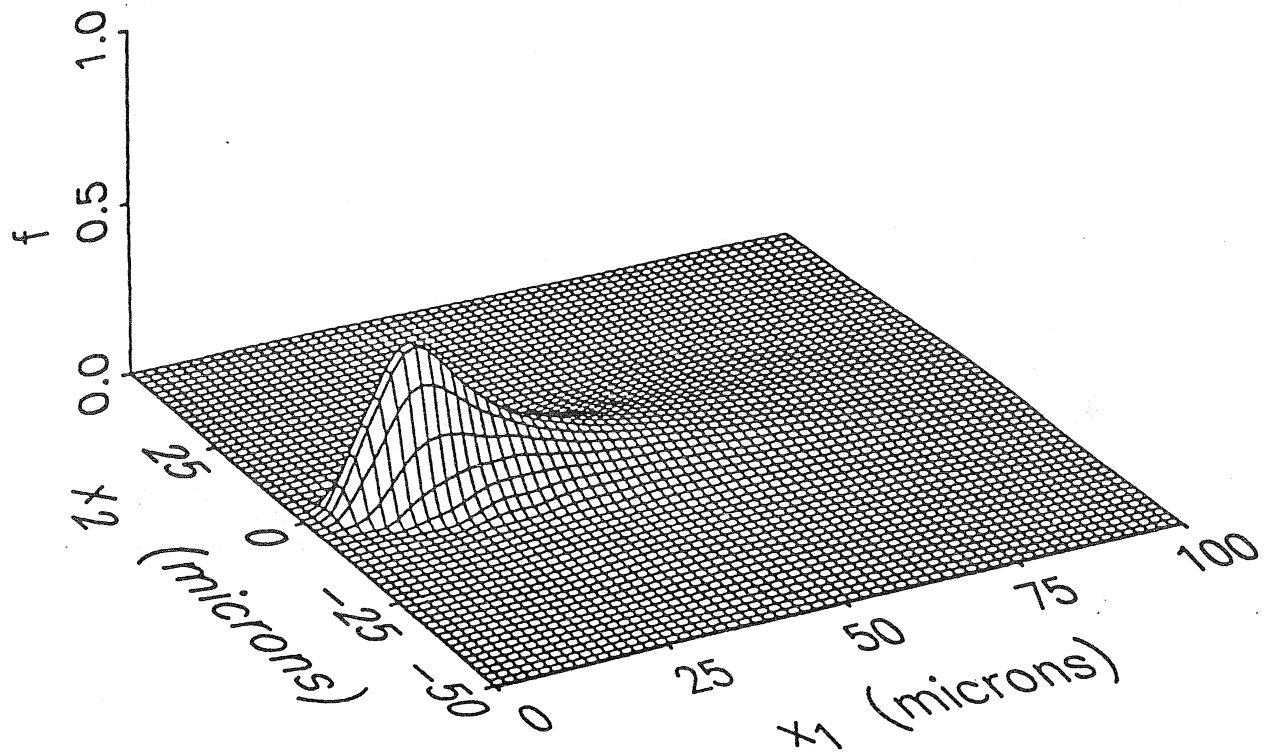


Fig. 6

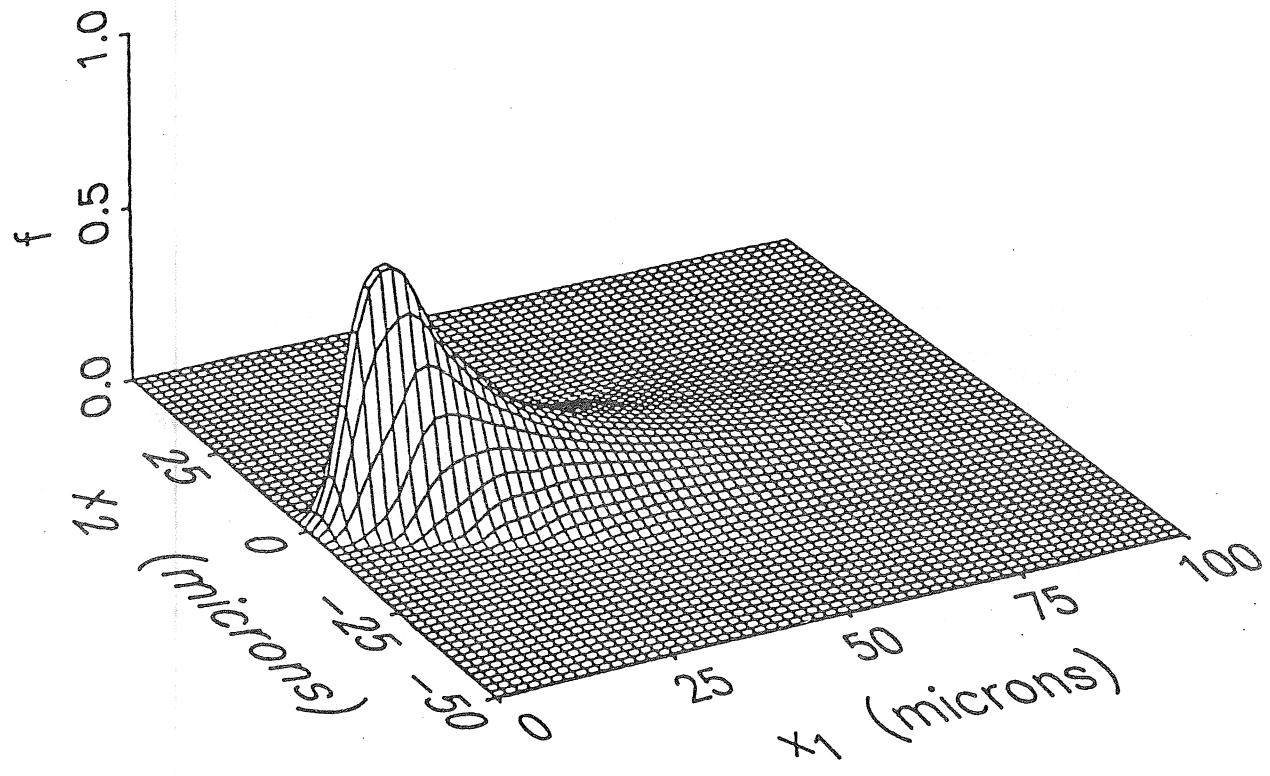


Fig. 7

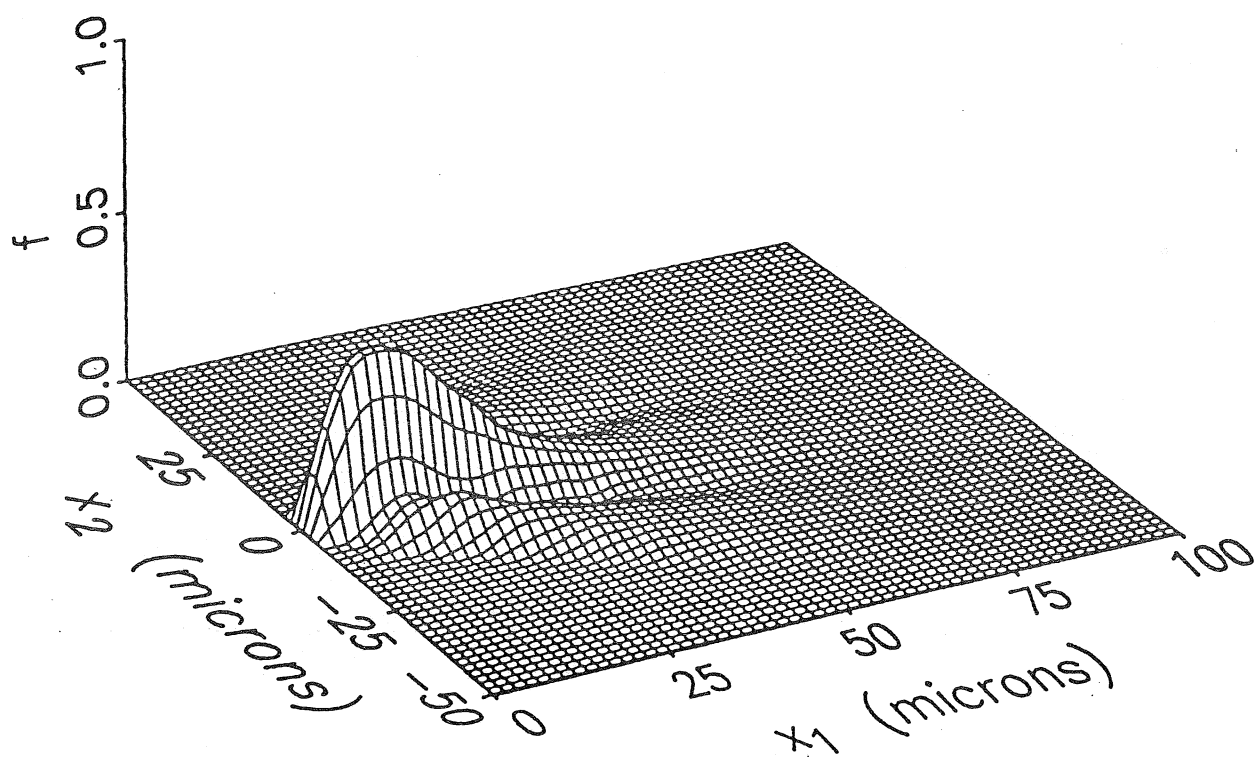


Fig. 8

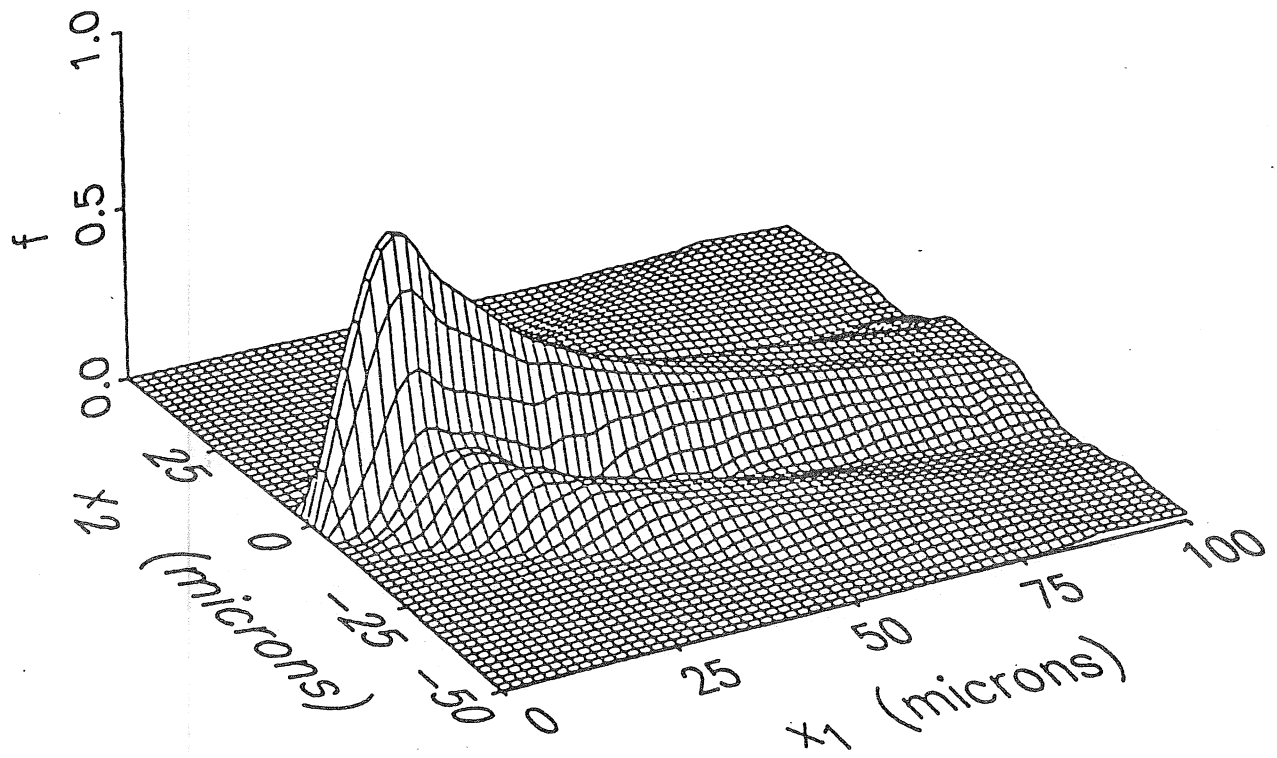


Fig. 9

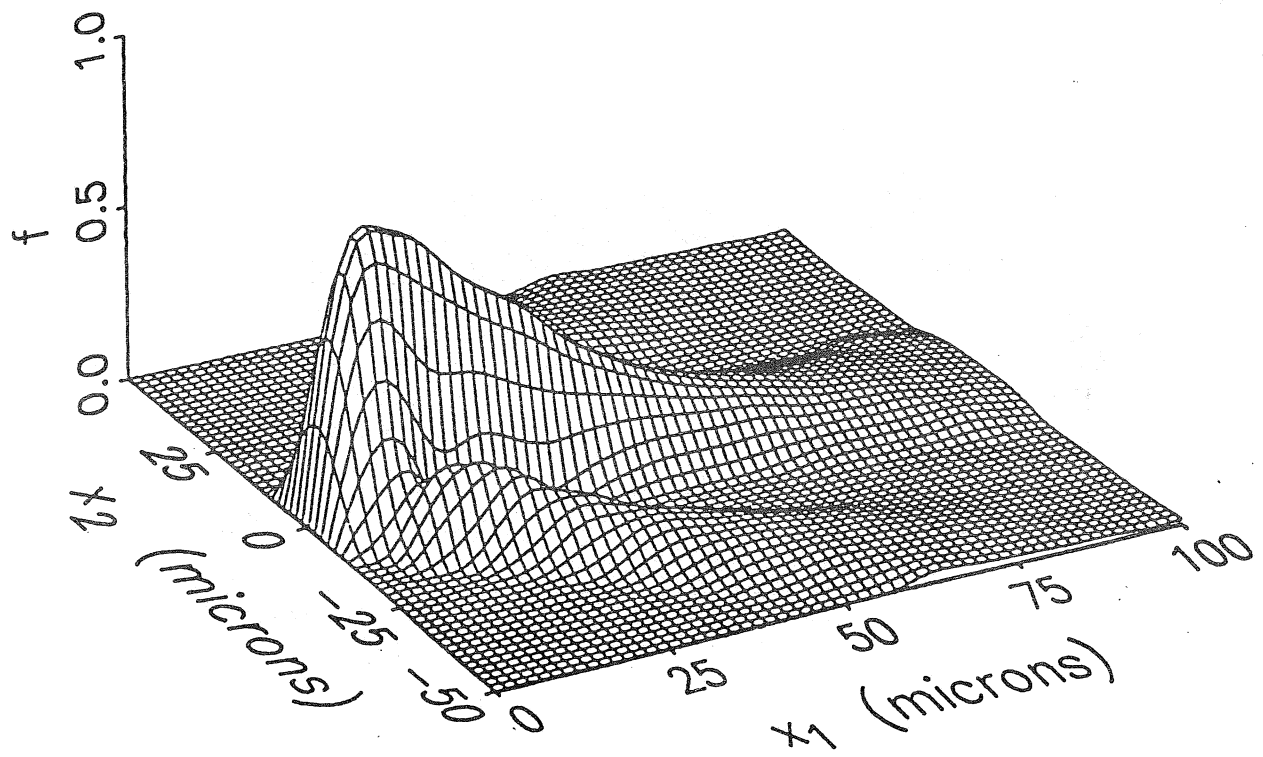


Fig. 10

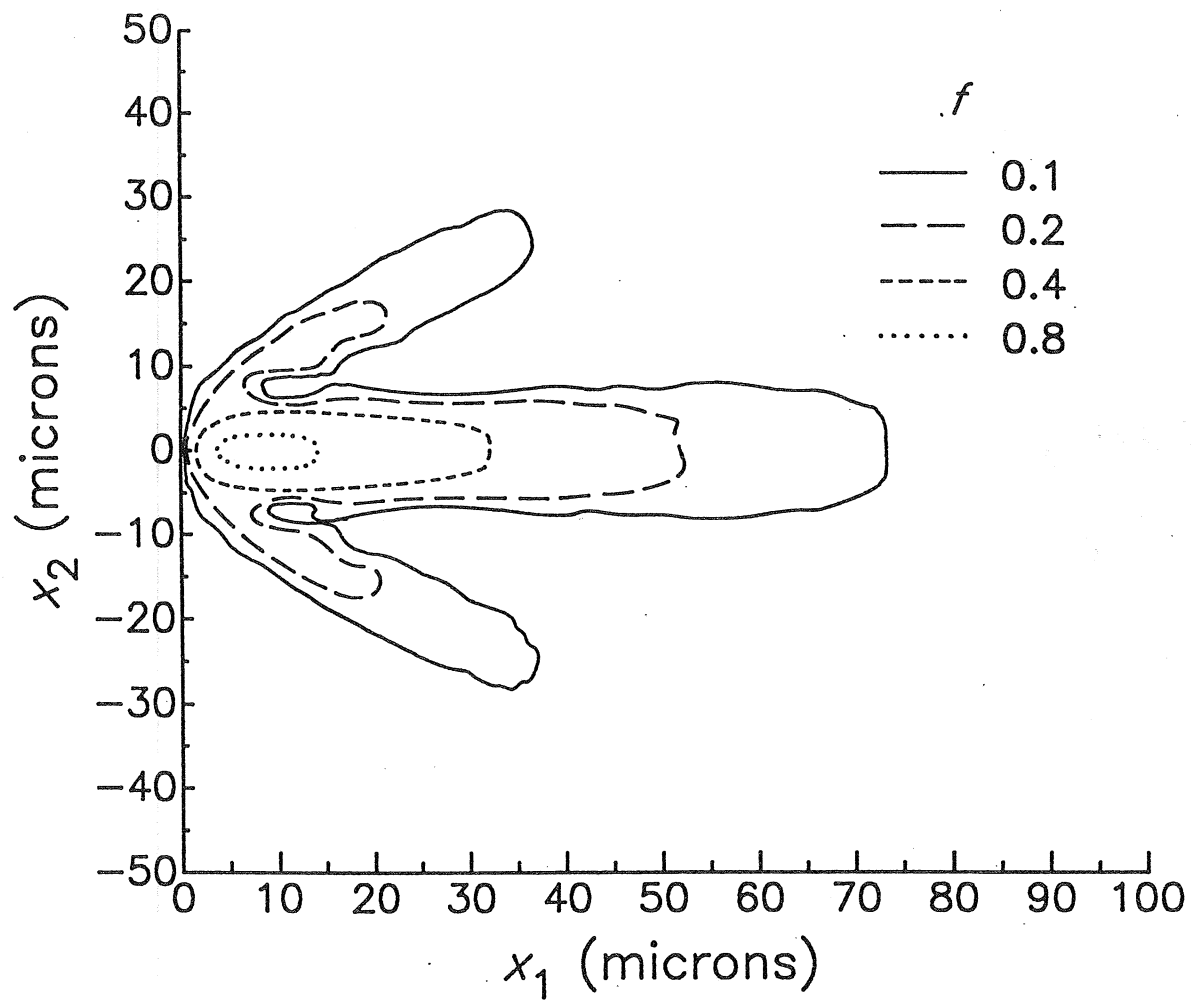


Fig. 11

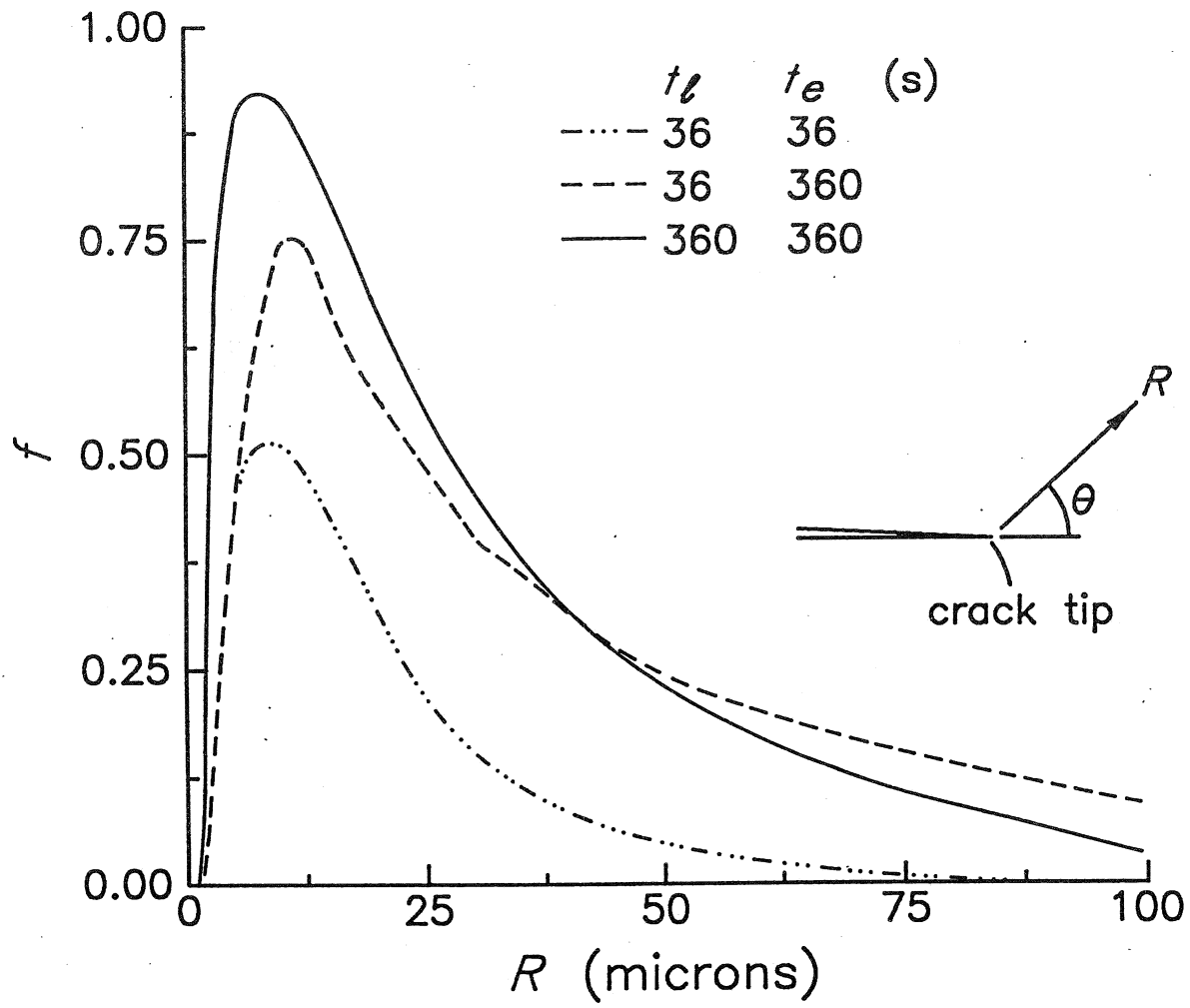


Fig. 12

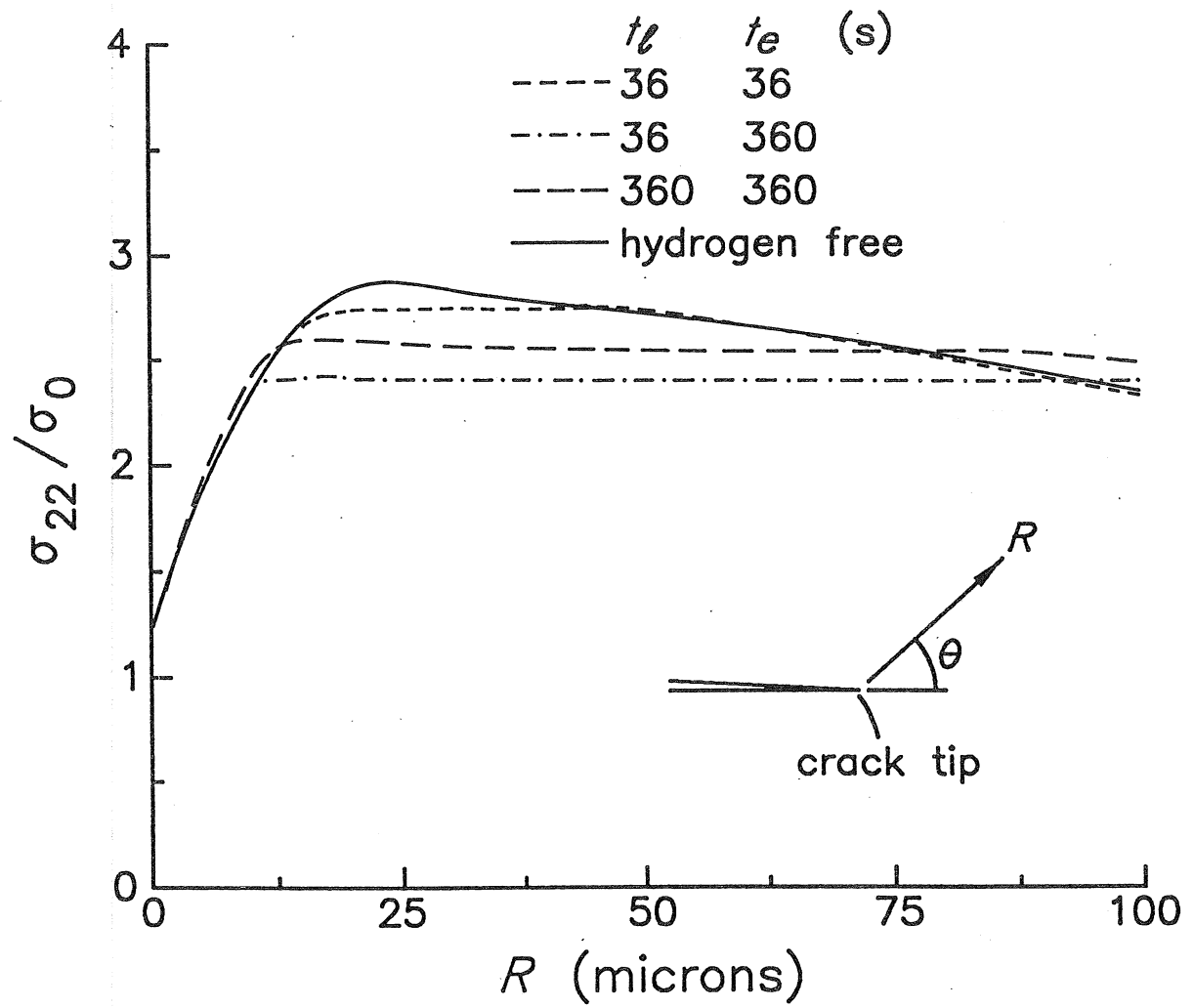


Fig. 13

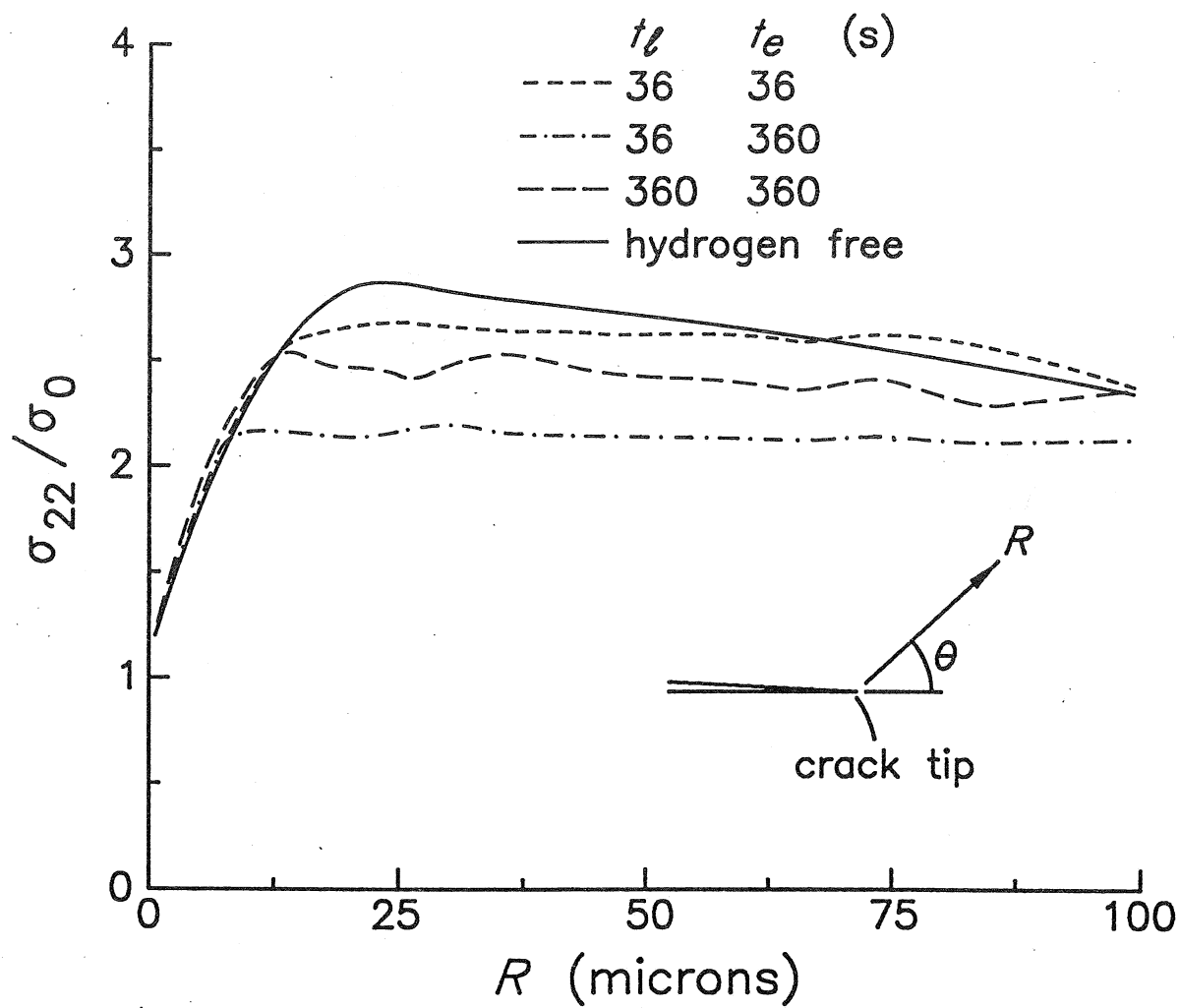


Fig. 14

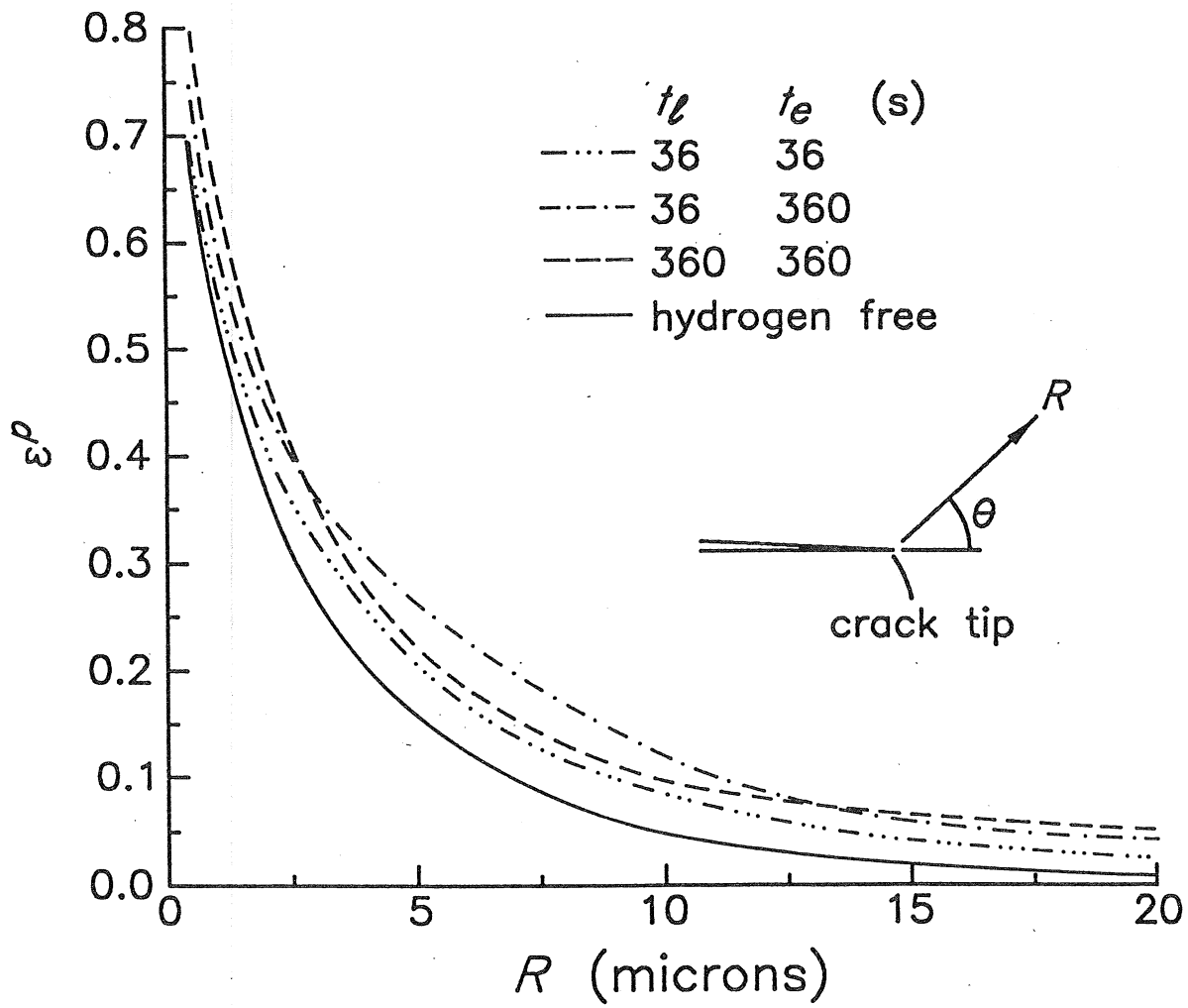


Fig. 15

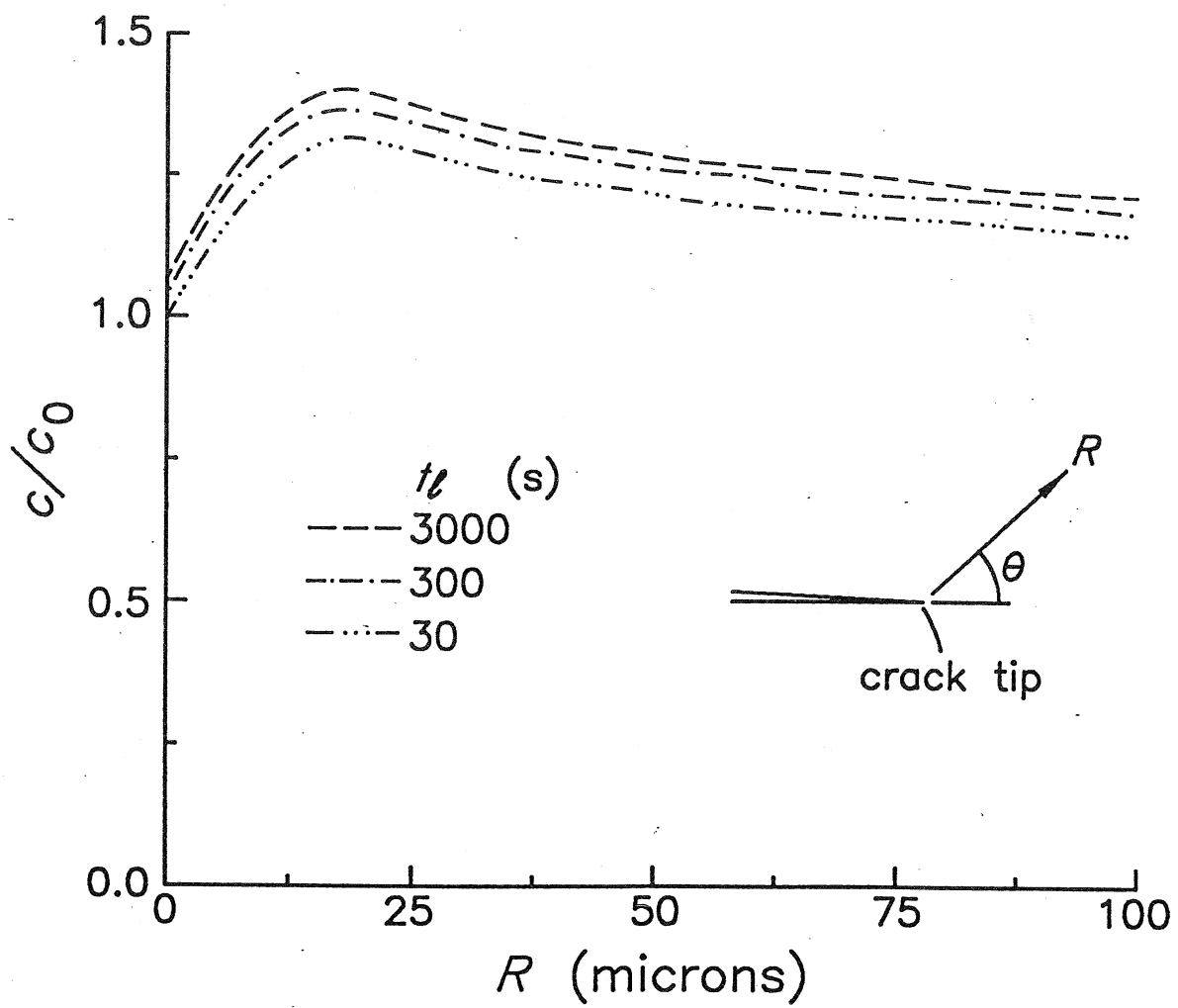


Fig. 16

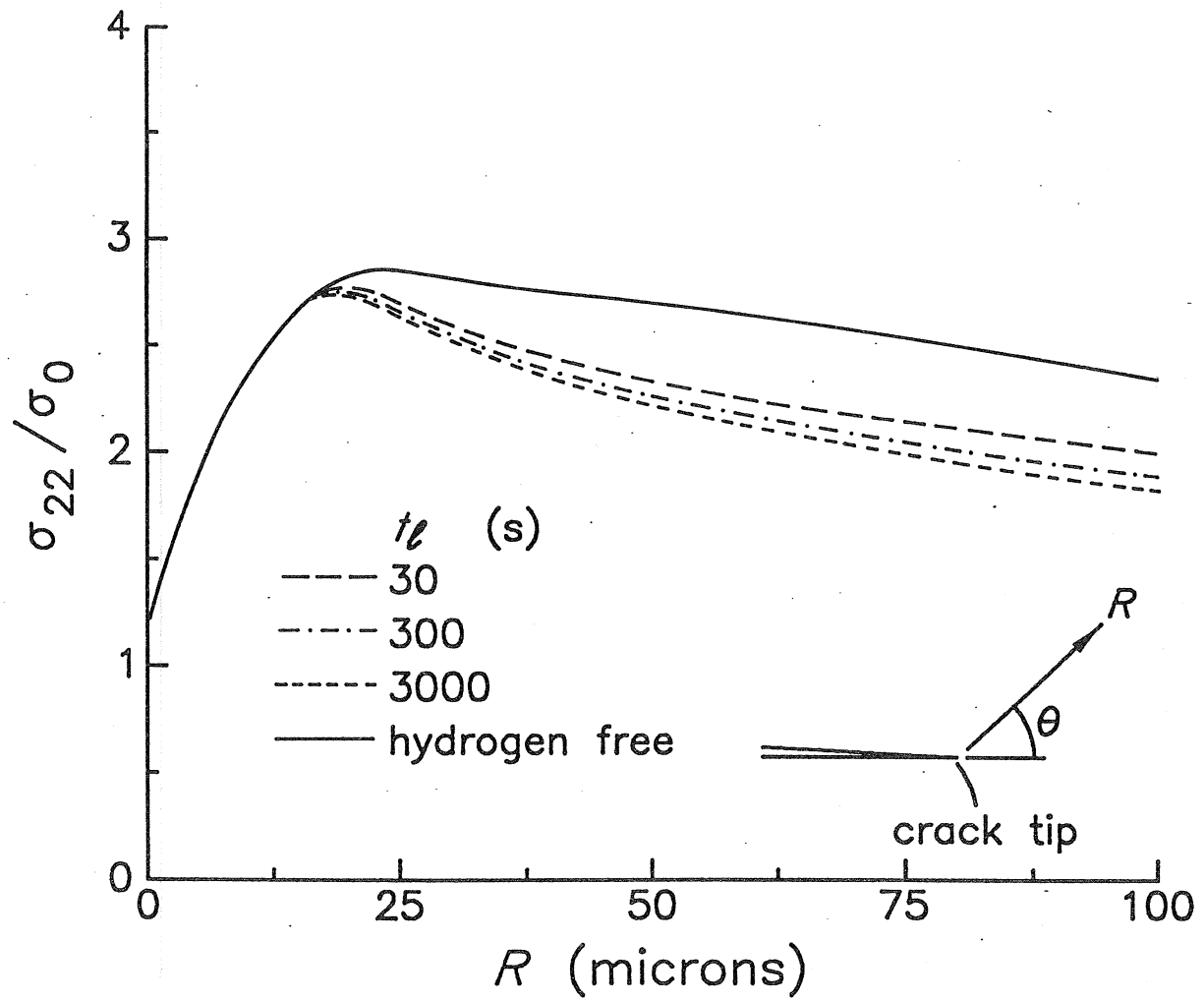


Fig. 17

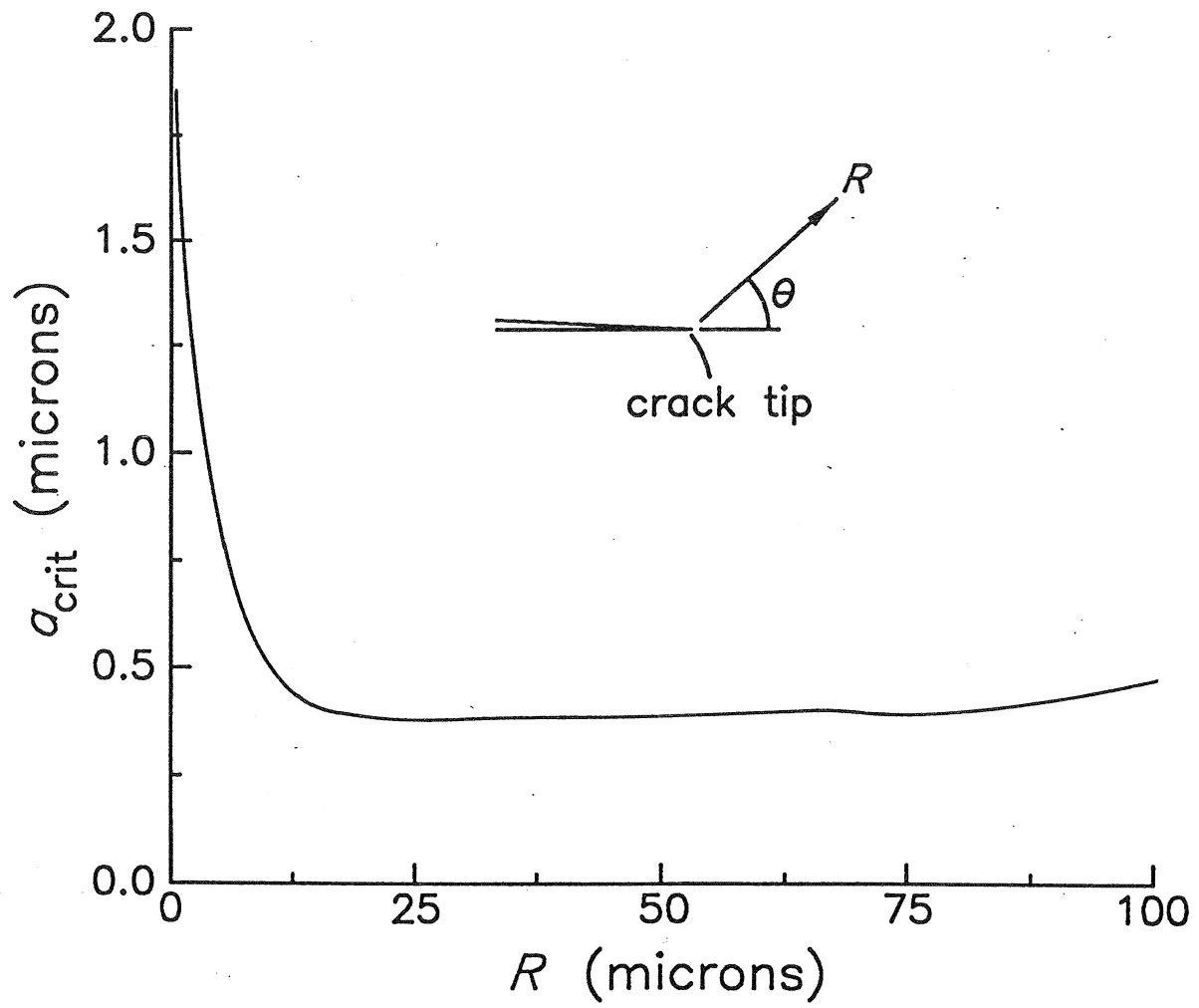


Fig. 18

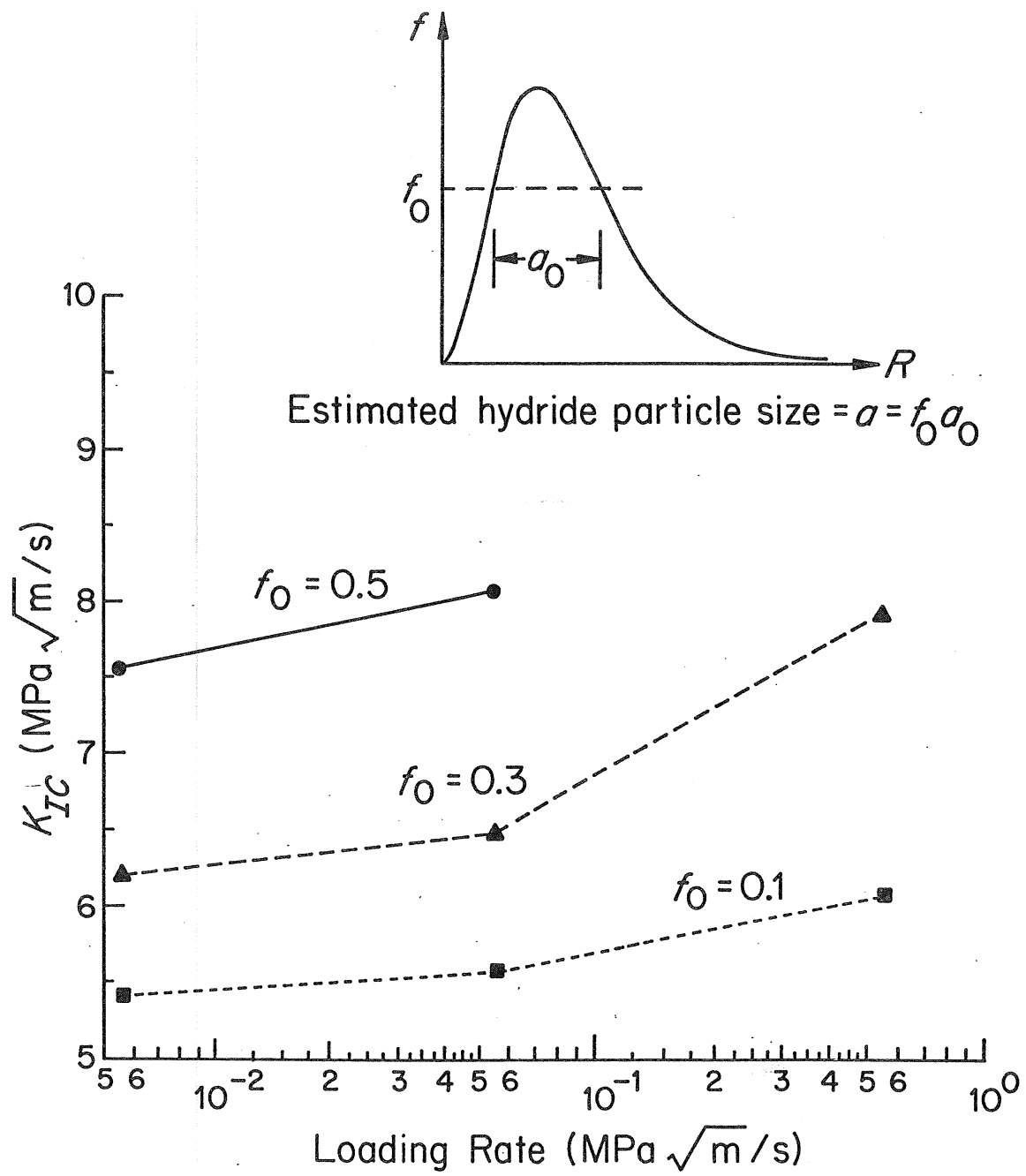


Fig. 19

List of Recent TAM Reports

No.	Authors	Title	Date
761	Balachandar, S., D. A. Yuen, and D. M. Reuteler	High Rayleigh number convection at infinite Prandtl number with temperature-dependent viscosity— <i>Geophysical and Astrophysical Fluid Dynamics</i> 83, 79–117 (1996)	July 1994
762	Phillips, J. W.	Arthur Newell Talbot—Proceedings of a conference to honor TAM's first department head and his family	Aug. 1994
763	Man., C. S., and D. E. Carlson	On the traction problem of dead loading in linear elasticity with initial stress— <i>Archive for Rational Mechanics and Analysis</i> 128, 223–247 (1994)	Aug. 1994
764	Zhang, Y., and R. L. Weaver	Leaky Rayleigh wave scattering from elastic media with random microstructures— <i>Journal of the Acoustical Society of America</i> 99, 88–99 (1996)	Aug. 1994
765	Cortese, T. A., and S. Balachandar	High-performance spectral simulation of turbulent flows in massively parallel machines with distributed memory— <i>International Journal of Supercomputer Applications</i> 9, 185–202 (1995)	Aug. 1994
766	Balachandar, S.	Signature of the transition zone in the tomographic results extracted through the eigenfunctions of the two-point correlation— <i>Geophysical Research Letters</i> 22, 1941–1944 (1995)	Sept. 1994
767	Piomelli, U.	Large-eddy simulation of turbulent flows	Sept. 1994
768	Harris, J. G., D. A. Rebinsky, and G. R. Wickham	An integrated model of scattering from an imperfect interface— <i>Journal of the Acoustical Society of America</i> 99, 1315–1325 (1996)	Sept. 1994
769	Hsia, K. J., and Z.-Q. Xu	The mathematical framework and an approximate solution of surface crack propagation under hydraulic pressure loading— <i>International Journal of Fracture</i> , in press (1996)	Sept. 1994
770	Balachandar, S.	Two-point correlation and its eigen-decomposition for optimal characterization of mantle convection	Oct. 1994
771	Lufrano, J. M., and P. Sofronis	Numerical analysis of the interaction of solute hydrogen atoms with the stress field of a crack— <i>International Journal of Solids and Structures</i> , 33, 1709–1723 (1996)	Oct. 1994
772	Aref, H., and S. W. Jones	Motion of a solid body through ideal fluid—Proceedings of the DCAMM 25th Anniversary Volume, 55–68 (1994)	Oct. 1994
773	Stewart, D. S., T. D. Aslam, J. Yao, and J. B. Bdzil	Level-set techniques applied to unsteady detonation propagation—In "Modeling in Combustion Science," <i>Lecture Notes in Physics</i> , eds. J. Buckmaster and J. Takeno 126, 390–409 (1996)	Oct. 1994
774	Mittal, R., and S. Balachandar	Effect of three-dimensionality on the lift and drag of circular and elliptic cylinders— <i>Physics of Fluids</i> 7, 1841–1865 (1995)	Oct. 1994
775	Stewart, D. S., T. D. Aslam, and J. Yao	On the evolution of cellular detonation	Nov. 1994 Revised Jan. 1996
776	Aref, H.	On the equilibrium and stability of a row of point vortices— <i>Journal of Fluid Mechanics</i> 290, 167–181 (1995)	Nov. 1994
777	Cherukuri, H. P., T. G. Shawki, and M. El-Raheb	An accurate finite-difference scheme for elastic wave propagation in a circular disk— <i>Journal of the Acoustical Society of America</i> , in press (1996)	Nov. 1994
778	Li, L., and N. R. Sottos	Improving hydrostatic performance of 1–3 piezocomposites— <i>Journal of Applied Physics</i> 77, 4595–4603 (1995)	Dec. 1994
779	Phillips, J. W., D. L. de Camara, M. D. Lockwood, and W. C. C. Grebner	Strength of silicone breast implants— <i>Plastic and Reconstructive Surgery</i> 97, 1215–1225 (1996)	Jan. 1995
780	Xin, Y.-B., K. J. Hsia, and D. A. Lange	Quantitative characterization of the fracture surface of silicon single crystals by confocal microscopy— <i>Journal of the American Ceramics Society</i> 78, 3201–3208 (1995)	Jan. 1995
781	Yao, J., and D. S. Stewart	On the dynamics of multi-dimensional detonation— <i>Journal of Fluid Mechanics</i> 309, 225–275 (1996)	Jan. 1995

List of Recent TAM Reports (cont'd)

No.	Authors	Title	Date
782	Riahi, D. N., and T. L. Sayre	Effect of rotation on the structure of a convecting mushy layer— <i>Acta Mechanica</i> 118 , 109–120 (1996)	Feb. 1995
783	Batchelor, G. K., and TAM faculty and students	A conversation with Professor George K. Batchelor	Feb. 1995
784	Sayre, T. L., and D. N. Riahi	Effect of rotation on flow instabilities during solidification of a binary alloy— <i>International Journal of Engineering Science</i> 34 , 1631–1645 (1996)	Feb. 1995
785	Xin, Y.-B., and K. J. Hsia	A technique to generate straight surface cracks for studying the dislocation nucleation condition in brittle materials— <i>Acta Metallurgica et Materialia</i> 44 , 845–853 (1996)	Mar. 1995
786	Riahi, D. N.	Finite bandwidth, long wavelength convection with boundary imperfections: Near-resonant wavelength excitation— <i>International Journal of Mathematics and Mathematical Sciences</i> , in press (1996)	Mar. 1995
787	Turner, J. A., and R. L. Weaver	Average response of an infinite plate on a random foundation— <i>Journal of the Acoustical Society of America</i> 99 , 2167–2175 (1996)	Mar. 1995
788	Weaver, R. L., and D. Sornette	The range of spectral correlations in pseudointegrable systems: GOE statistics in a rectangular membrane with a point scatterer— <i>Physical Review E</i> 52 , 341 (1995)	Apr. 1995
789	Students in TAM 293– 294	Thirty-second student symposium on engineering mechanics, J. W. Phillips, coordinator: Selected senior projects by K. F. Anderson, M. B. Bishop, B. C. Case, S. R. McFarlin, J. M. Nowakowski, D. W. Peterson, C. V. Robertson, and C. E. Tsoukatos	Apr. 1995
790	Figa, J., and C. J. Lawrence	Linear stability analysis of a gravity-driven Newtonian coating flow on a planar incline	May 1995
791	Figa, J., and C. J. Lawrence	Linear stability analysis of a gravity-driven viscosity-stratified Newtonian coating flow on a planar incline	May 1995
792	Cherukuri, H. P., and T. G. Shawki	On shear band nucleation and the finite propagation speed of thermal disturbances— <i>International Journal of Solids and Structures</i> , in press (1996)	May 1995
793	Harris, J. G.	Modeling scanned acoustic imaging of defects at solid interfaces—Chapter in <i>IMA Workshop on Inverse Problems in Wave Propagation</i> , eds. G. Chevant, G. Papanicolaou, P. Sacks and W. E. Symes, 237–258, Springer-Verlag, New York (1996)	May 1995
794	Sottos, N. R., J. M. Ockers, and M. J. Swindeman	Thermoelastic properties of plain weave composites for multilayer circuit board applications	May 1995
795	Aref, H., and M. A. Stremler	On the motion of three point vortices in a periodic strip— <i>Journal of Fluid Mechanics</i> 314 , 1–25 (1996)	June 1995
796	Barenblatt, G. I., and N. Goldenfeld	Does fully-developed turbulence exist? Reynolds number independence versus asymptotic covariance— <i>Physics of Fluids</i> 7 , 3078–3082 (1995)	June 1995
797	Aslam, T. D., J. B. Bdzil, and D. S. Stewart	Level set methods applied to modeling detonation shock dynamics— <i>Journal of Computational Physics</i> , 126 , 390–409 (1996)	June 1995
798	Nimmagadda, P. B. R., and P. Sofronis	The effect of interface slip and diffusion on the creep strength of fiber and particulate composite materials— <i>Proceedings of the ASME Applied Mechanics Division</i> 213 , 125–143 (1995)	July 1995
799	Hsia, K. J., T.-L. Zhang, and D. F. Socie	Effect of crack surface morphology on the fracture behavior under mixed mode loading— <i>ASTM Special Technical Publication</i> 1296, in press (1996)	July 1995
800	Adrian, R. J.	Stochastic estimation of the structure of turbulent fields— <i>Eddy Structure Identification</i> , ed. J. P. Bonnet, Springer: Berlin 145–196 (1996)	Aug. 1995
801	Riahi, D. N.	Perturbation analysis and modeling for stratified turbulence	Aug. 1995

List of Recent TAM Reports (cont'd)

No.	Authors	Title	Date
802	Thoroddsen, S. T.	Conditional sampling of dissipation in high Reynolds number turbulence— <i>Physics of Fluids</i> 8, 1333–1335	Aug. 1995
803	Riahi, D. N.	On the structure of an unsteady convecting mushy layer— <i>Acta Mechanica</i> , in press (1996)	Aug. 1995
804	Meleshko, V. V.	Equilibrium of an elastic rectangle: The Mathieu–Inglis–Pickett solution revisited— <i>Journal of Elasticity</i> 40, 207–238 (1995)	Aug. 1995
805	Jonnalagadda, K., G. E. Kline, and N. R. Sottos	Local displacements and load transfer in shape memory alloy composites	Aug. 1995
806	Nimmagadda, P. B. R., and P. Sofronis	On the calculation of the matrix–reinforcement interface diffusion coefficient in composite materials at high temperatures— <i>Acta Metallurgica et Materialia</i> , 44, 2711–2716 (1996)	Aug. 1995
807	Carlson, D. E., and D. A. Tortorelli	On hyperelasticity with internal constraints— <i>Journal of Elasticity</i> 42, 91–98 (1966)	Aug. 1995
808	Sayre, T. L., and D. N. Riahi	Oscillatory instabilities of the liquid and mushy layers during solidification of alloys under rotational constraint— <i>Acta Mechanica</i> , in press (1996)	Sept. 1995
809	Xin, Y.-B., and K. J. Hsia	Simulation of the brittle–ductile transition in silicon single crystals using dislocation mechanics	Oct. 1995
810	Ulysse, P., and R. E. Johnson	A plane-strain upper-bound analysis of unsymmetrical single-hole and multi-hole extrusion processes	Oct. 1995
811	Fried, E.	Continua described by a microstructural field— <i>Zeitschrift für angewandte Mathematik und Physik</i> , 47, 168–175 (1996)	Nov. 1995
812	Mittal, R., and S. Balachandar	Autogeneration of three-dimensional vortical structures in the near wake of a circular cylinder	Nov. 1995
813	Segev, R., E. Fried, and G. de Botton	Force theory for multiphase bodies— <i>Journal of Geometry and Physics</i> , in press (1996)	Dec. 1995
814	Weaver, R. L.	The effect of an undamped finite-degree-of-freedom “fuzzy” substructure: Numerical solutions and theoretical discussion— <i>Journal of the Acoustical Society of America</i> 100, 3159–3164 (1996)	Jan. 1996
815	Haber, R. B., C. S. Jog, and M. P. Bendsøe	A new approach to variable-topology shape design using a constraint on perimeter— <i>Structural Optimization</i> 11, 1–12 (1996)	Feb. 1996
816	Xu, Z.-Q., and K. J. Hsia	A numerical solution of a surface crack under cyclic hydraulic pressure loading	Mar. 1996
817	Adrian, R. J.	Bibliography of particle velocimetry using imaging methods: 1917–1995— <i>Produced and distributed in cooperation with TSI, Inc., St. Paul, Minn.</i>	Mar. 1996
818	Fried, E., and G. Grach	An order-parameter based theory as a regularization of a sharp-interface theory for solid–solid phase transitions— <i>Archive for Rational Mechanics and Analysis</i> , in press (1996)	Mar. 1996
819	Vonderwell, M. P., and D. N. Riahi	Resonant instability mode triads in the compressible boundary-layer flow over a swept wing— <i>Physics of Fluids</i> , in press (1996)	Mar. 1996
820	Short, M., and D. S. Stewart	Low-frequency two-dimensional linear instability of plane detonation— <i>Journal of Fluid Mechanics</i> , in press (1997)	Mar. 1996
821	Casagrande, A., and P. Sofronis	On the scaling laws for the consolidation of nanocrystalline powder compacts— <i>Proceedings of the IUTAM Symposium on the Mechanics of Granular and Porous Materials</i> (1996)	Apr. 1996
822	Xu, S., and D. S. Stewart	Deflagration-to-detonation transition in porous energetic materials: A comparative model study— <i>Journal of Fluid Mechanics</i> , in press (1997)	Apr. 1996
823	Weaver, R. L.	Mean and mean-square responses of a prototypical master/fuzzy structure— <i>Journal of the Acoustical Society of America</i> , in press (1996)	Apr. 1996
824	Fried, E.	Correspondence between a phase-field theory and a sharp-interface theory for crystal growth— <i>Continuum Mechanics and Thermodynamics</i> , in press (1997)	Apr. 1996

List of Recent TAM Reports (cont'd)

No.	Authors	Title	Date
825	Students in TAM 293-294	Thirty-third student symposium on engineering mechanics, J. W. Phillips, coordinator: Selected senior projects by W. J. Fortino II, A. A. Mordock, and M. R. Sawicki	May 1995
826	Riahi, D. N.	Effects of roughness on nonlinear stationary vortices in rotating disk flows— <i>Mathematical and Computer Modeling</i> , in press (1996)	June 1996
827	Riahi, D. N.	Nonlinear instabilities of shear flows over rough walls	June 1996
828	Weaver, R. L.	Multiple scattering theory for a plate with sprung masses: Mean and mean-square responses	July 1996
829	Moser, R. D., M. M. Rogers, and D. W. Ewing	Self-similarity of time-evolving plane wakes	July 1996
830	Lufrano, J. M., and P. Sofronis	Enhanced hydrogen concentrations ahead of rounded notches and cracks—Competition between plastic strain and hydrostatic constraint	July 1996
831	Riahi, D. N.	Effects of surface corrugation on primary instability modes in wall-bounded shear flows	Aug. 1996
832	Bechel, V. T., and N. R. Sottos	Measuring debond length in the fiber pushout test—Proceedings of the ASME Mechanics and Materials Conference (1996)	Aug. 1996
833	Riahi, D. N.	Effect of centrifugal and Coriolis forces on chimney convection during alloy solidification— <i>Journal of Crystal Growth</i> , in press (1997)	Sept. 1996
834	Cermelli, P., and E. Fried	The influence of inertia on configurational forces in a deformable solid— <i>Proceedings of the Royal Society of London A</i> , in press (1996)	Oct. 1996
835	Riahi, D. N.	On the stability of shear flows with combined temporal and spatial imperfections	Oct. 1996
836	Carranza, F. L., B. Fang, and R. B. Haber	An adaptive space-time finite element model for oxidation-driven fracture	Nov. 1996
837	Carranza, F. L., B. Fang, and R. B. Haber	A moving cohesive interface model for fracture in creeping materials	Nov. 1996
838	Balachandar, S., R. Mittal, and F. M. Najjar	Properties of the mean wake recirculation region in two-dimensional bluff body wakes	Dec. 1996
839	Ti, B. W., W. D. O'Brien, Jr., and J. G. Harris	Measurements of coupled Rayleigh wave propagation in an elastic plate	Dec. 1996
840	Phillips, W. R. C.	On finite-amplitude rotational waves in viscous shear flows	Jan. 1997
841	Riahi, D. N.	Direct resonance analysis and modeling for a turbulent boundary layer over a corrugated surface	Jan. 1997
842	Liu, Z. C., R. J. Adrian, C. D. Meinhart, and W. Lai	Structure of a turbulent boundary layer using a stereoscopic, large format video-PIV	Jan. 1997
843	Fang, B., F. L. Carranza, and R. B. Haber	An adaptive discontinuous Galerkin methods for viscoplastic analysis	Jan. 1997
844	Xu, S., T. D. Aslam, and D. S. Stewart	High-resolution numerical simulation of ideal and non-ideal compressible reacting flows with embedded internal boundaries	Jan. 1997
845	Zhou, J., C. D. Meinhart, S. Balachandar, and R. J. Adrian	Formation of coherent hairpin packets in wall turbulence	Feb. 1997
846	Lufrano, J. M., P. Sofronis, and H. K. Birnbaum	Elastoplastically accommodated hydride formation and embrittlement	Feb. 1997